Berkeley-RWAWC: a new CYGNSS-based watermask unveils unique observations of seasonal dynamics in the Tropics

Tianjiao Pu[1], Cynthia Gerlein-Safdi[1], Ying Xiong[2], Mengze Li[2,3], Eric A. Kort[2], Anthony Bloom[4]

[1]Dept. of Civil and Environmental Engineering, UC Berkeley, Berkeley, CA, USA
[2]Dept. of Climate and Space Sciences and Engineering, University of Michigan, Ann Arbor, MI, USA
[3]Dept. of Earth System Science, Stanford University, Palo Alto, CA, USA
[4]Jet Propulsion Laboratory, Pasadena, CA, USA

Key Points:

- Vegetation and clouds can obstruct the view of waterbodies, making accurate, seasonal mapping difficult
- This new CYGNSS-based product combines L-band microwaves with computer vision to produce quasi-global monthly maps of waterbodies
- The product shows greater seasonal and interannual variability than other datasets for new insights into Tropical hydrological processes

Corresponding author: Tianjiao Pu, putianjiao@berkeley.edu

Abstract

The UC Berkeley Random Walk Algorithm WaterMask from CYGNSS (Berkeley-RWAWC) is a new data product designed to address the challenges of monitoring inundation in regions hindered by dense vegetation and cloud cover as is the case in most of the Tropics. The Cyclone Global Navigation Satellite System (CYGNSS) constellation provides data with a higher temporal repeat frequency compared to single-satellite systems, offering the potential for generating moderate spatial resolution inundation maps with improved temporal resolution while having the capability to penetrate clouds and vegetation. This paper details the development of a computer vision algorithm for inundation mapping over the entire CYGNSS domain (37.4°N to 37.4°S). The unique reliance on CYGNSS data sets our method apart in the field, highlighting CYGNSS's indication of water existence. Berkeley-RWAWC provides monthly, near-real-time inundation maps starting in August 2018 and across the CYGNSS latitude range, with a spatial resolution of $0.01^\circ \times 0.01^\circ$. Here we present our workflow and parameterization strategy, alongside a comparative analysis with established surface water datasets (SWAMPS, WAD2M) in four regions: the Amazon Basin, the Pantanal, the Sudd, and the Indo-Gangetic Plain. The comparisons reveal Berkeley-RWAWC's enhanced capability to detect seasonal variations, demonstrating its usefulness in studying tropical wetland hydrology. We also discuss potential sources of uncertainty and reasons for variations in inundation retrievals. Berkeley-RWAWC represents a valuable addition to environmental science, offering new insights into tropical wetland dynamics.

Plain Language Summary

The UC Berkeley Random Walk Algorithm WaterMask from CYGNSS (Berkeley-RWAWC) is a new data product developed to better monitor areas that are hard to observe due to thick vegetation and clouds, such as tropical regions. Using data from the Cyclone Global Navigation Satellite System (CYGNSS), an 8-satellite constellation, Berkeley-RWAWC has more frequent data collection compared to single-satellite systems. This allows mapping of flooding or water accumulation with improved accuracy over time, even in clouds-prone and overgrown areas. Berkeley-RWAWC spans from 37.4° North to 37.4° South and consists of monthly inundation maps at approximately 1 km by 1km resolution since August 2018. The method places the greatest emphasis on CYGNSS data indications of where is the water, making it different from others. In this paper, we explain how we made the maps, and compare them with other datasets in four different areas: the Amazon Basin, the Pantanal, the Sudd, and the Indo-Gangetic Plain. Our comparisons show that Berkeley-RWAWC is better at showing how water changes with the seasons, which is useful for understanding tropical wetland water cycles. Berkeley-RWAWC is publicly available and can become an important new resource for studying our planet, especially in the study of patterns in tropical wetlands.

1 Introduction

1.1 Hydrological Challenges by Climate Change

In the realm of Earth's terrestrial hydrology, comprehensively capturing the spatial distribution and temporal dynamics of global inland water has been a long-standing scientific pursuit (Finlayson & Spiers, 1999; Prigent et al., 2001; Fekete et al., 2002; Lehner & Döll, 2004; Prigent et al., 2007; Lehner et al., 2008; Wood et al., 2011; Pekel et al., 2016; Jensen & Mcdonald, 2019; Prigent et al., 2020). This pursuit is now more critical than ever due to climate change, driven by increased greenhouse gas emissions (GHG) (IPCC, 2023), which is fundamentally reshaping the global distribution of water (Konapala et al., 2020). The shifts are happening now and at an ever-increasing pace (Thiery et al., 2021), causing an upsurge in extreme events like floods and droughts across the globe (Betts et al., 2018; Lange et al.,

2020), in turn disrupting various natural ecosystems that have long been adapted to the ebb and flow of natural variability they experienced (Trenberth et al., 2015).

While the developed world bears substantial responsibility for the anthropogenic greenhouse gas emissions fueling climate change (Mgbemene et al., 2016; Dong et al., 2019), the disproportional impact is most keenly experienced by the tropical regions, where a significant portion of the developing world resides (UNESCO, 2020). Developing regions, constrained by limited financial resources and governance capacity for effective adaptation and mitigation, are particularly vulnerable to climate-related shocks (Das Gupta, 2014). Understanding the dynamics of water distribution and its variations over time is vital for scientific, environmental, and humanistic applications. This knowledge is crucial for population preparedness in adapting to changing water availability while safeguarding natural ecosystems, their services, and the biodiversity they contain.

1.2 Knowledge Gap on Tropical Wetlands

Remote sensing techniques have been instrumental in facilitating the observation of tropical water, offering an unparalleled global perspective over the course of decades (Alsdorf et al., 2007; Palmer et al., 2015; Topp et al., 2020). Various platforms are employed for water detection, ranging from optical sensors like Landsat (Masek et al., 2020) to near-infrared (NIR) instruments such as MODIS (Justice et al., 2002), and microwave missions like SMAP (Entekhabi et al., 2010). Landsat, renowned for its remarkable 30-meter spatial resolution, is one of the premier data sources for water body monitoring (Pekel et al., 2016). However, despite the extensive scope of remote sensing observations, knowledge gaps persist in hydrological monitoring in the tropics, particularly in terms of its seasonal and inter-seasonal patterns. Indeed, cloud cover and dense canopies are the two major challenges for obtaining valid optical and near-infrared observations. In tropical rainforests, the rainy season often entails extended periods of persistent cloud cover, sometimes lasting for multiple consecutive months (Martins et al., 2018). Additionally, the presence of dense vegetation and canopies, particularly along the fringes of large water bodies and sometimes even fully concealing small water bodies entirely, further obscured valid observations.

As a consequence, most tropical water maps tend to underestimate the actual extent of these waterbodies, displaying a bias toward representing dry season conditions, which often represent only a fraction of the maximum extent during the peak of the rainy season. This raises a pressing concern related to the quantification of the impact of inland waterbodies and wetlands in particular within the context of climate change. Wetlands represent Earth's largest natural source of methane emissions, as well-documented (Saunois et al., 2020), yet paradoxically, one of the most uncertain, due to limitations in the quality of wetland extent data (Parker et al., 2018). Of particular importance are tropical wetlands, as they contribute substantially more methane compared to their high-latitude counterparts (Z. Zhang et al., 2017). Meanwhile, within tropical regions, up to 80% of the uncertainty in wetland emissions of methane (CH_4) can be associated with the uncertainties in wetland extent (Bloom et al., 2017). Thus, it becomes crucial for accurately characterizing the spatial extent and temporal variations in inundation and aquatic habitats (Melack et al., 2022).

1.3 Filling the Gap with spaceborne GNSS-R Technique

To overcome these constraints, recent studies have embraced microwave remote sensing tools, which provide superior cloud penetration capabilities and are less influenced by dense vegetation. Coarse spatial resolution radiometer datasets, with a resolution greater than 25 kilometers, provide a wealth of temporally rich observations. Notable inundation products include GIEMS-2 (Prigent et al., 2020), which provides monthly data, and SWAMPSv3 (Jensen & Mcdonald, 2019), delivering daily information. On the other hand, high spatial resolution synthetic aperture radar (SAR) datasets, with resolutions of less than 100 meters, offer detailed observations but limited temporal coverage. For instance, Sentinel-1 SAR

currently has a revisit frequency of 6–12 days, and the upcoming NASA-ISRO Synthetic Aperture Radar (NISAR) mission is expected to provide a similar revisit frequency (Kellogg et al., 2020).

Thus, existing microwave-based inundation products necessitate trade-offs between spatial and temporal resolution. The Global Navigation Satellite System Reflectometry (GNSS-R) technology emerged with great potential for filling the gap. GNSS is a collective term encompassing satellite constellations that offer global or regional positioning, navigation, and timing (PNT) services. Presently, these systems include the United States' Global Positioning System (GPS), Russian Global'naya Navigatsionnaya Sputnikova Sistema (GLONASS), the European Galileo system, the Chinese BeiDou System (BDS), the Japanese Quasi-Zenith Satellite System (QZSS), and the Indian Regional Navigation Satellite System (IRNSS/NavIC). The basic principle of GNSS-R involves receiving signals transmitted from these navigation satellites and measuring the changes in the signals' properties as they interact with the Earth's surface (Gleason et al., 2005).

Launched in December 2016, the Cyclone Global Navigation Satellite System (CYGNSS) is the first space-based GNSS-R constellation system that focuses on tropical cyclones and tropical convection. Originally conceived to address the urgent demand for better hurricane intensity forecasts, CYGNSS allows for high-resolution wind measurements under extreme conditions such as heavy rain and intense winds, and offers a high revisit frequency, as evidenced by statistical distributions indicating a median revisit time of 2.8 hours and a mean revisit time of 7.2 hours (C. S. Ruf, 2022). Furthermore, GNSS-R technique, being "receiver only", eliminates the need for a transmitter, substantially lowering sensor power requirements compared to traditional scatterometers (C. S. Ruf et al., 2016), therefore significantly reducing the cost of these missions compared to active microwave satellites.

Beyond its primary mission, CYGNSS data has demonstrated remarkable sensitivity to inland water. GPS satellites, operating at 1.575 GHz in the L-band, can penetrate clouds, rain, and dense vegetation canopies, while also offering strong signals through coherent specular scattering when in contact with calm water surfaces, setting them apart from the diffuse scattering in the surroundings (C. S. Ruf et al., 2018). The bi-static radar geometry also appears to contribute to CYGNSS' high sensitivity to inland waters, allowing for better sensitivity to small waterways than SAR (Downs et al., 2023). Distinguished by rapid data acquisition capabilities, high revisit frequency, cost-effectiveness, extensive coverage spanning approximately 38°S to 38°N, and enduring mission longevity, CYGNSS data has emerged as a transformative asset in the field of hydrological remote sensing.

2 Background

2.1 Existing WaterMasks

2.1.1 SWAMPS

The Surface Water Microwave Product Series (SWAMPS) is a coarse-resolution ($\sim$ 25 km) global inundated area fraction dataset derived from both active and passive microwave remote sensing. This dataset incorporates data from sources such as SSM/I, SSMIS, ERS, QuikSCAT, and ASCAT (Jensen & Mcdonald, 2019), and exhibits wetlands, rivers, lakes, reservoirs, rice paddies, and areas that experience episodic inundation. SWAMPS stands out as one of the most extensive microwave remote sensing datasets available for download, offering daily data files that cover the period from 2000 to 2020.

2.1.2 WAD2M

The Monthly global dataset of Wetland Area and Dynamics for Methane Modeling (WAD2M) is a derivative of SWAMPS, incorporating additional active and passive microwave remote sensing products (Z. Zhang et al., 2021b). This dataset is specifically

designed to capture the spatiotemporal dynamics of both inundated and non-inundated vegetated wetlands, removing lakes, ponds, rice paddies, and rivers. WAD2M offers a spatial resolution of 25km and covers the time frame from 2000 to 2020.

2.2 CYGNSS

There is an ever-growing interest in employing CYGNSS data to retrieve geophysical variables related to terrestrial hydrology. This burgeoning field has not only prompted extensive research but has also led to the development of additional GNSS-R missions by governmental agencies and private companies. Research investigations have been conducted to assess CYGNSS's capacity for mapping inland surface water with different approaches e.g., (C. Chew et al., 2018; Gerlein-Safdi & Ruf, 2019; Morris et al., 2019; Wan et al., 2019; Al-Khaldi et al., 2021; Li et al., 2021; S. Zhang et al., 2021; Chapman et al., 2022; Zeiger et al., 2022; Downs et al., 2023). Furthermore, a capacity for detecting near-surface soil moisture sensitivity was also recognized e.g., (C. C. Chew & Small, 2018; Kim & Lakshmi, 2018; Al-Khaldi et al., 2019; Clarizia et al., 2019; Eroglu et al., 2019; Senyurek et al., 2020; Yan et al., 2020). Presently, there exist several GNSS-R missions in development, undertaken by both governmental agencies (e.g., ESA's HydroGNSS mission, as detailed by (Unwin et al., 2021)) and private companies (e.g., Spire and Muon Space), all with the shared goal of retrieving hydrological data.

2.2.1 Existing Products

Currently, the only CYGNSS-based, publicly available data product is the UCAR/CU CYGNSS inundation product, which is generated at a spatial resolution of 3×3 km with a temporal resolution of three days, covering CYGNSS's entire observational range (within $\pm$ 38° latitude) as detailed in the study by (C. Chew et al., 2023). The study introduced a retrieval algorithm specifically tailored for mapping fractional inundation, utilizing CYGNSS data as the primary input to a parameterized reflectivity model. The product provides a wealth of insightful information. Nevertheless, it is worth noting the uncertainties associated with this approach are primarily rooted in the parameterization of soil moisture and water surface roughness, which tend to result in an underestimation of fractional inundation, especially in regions featuring extensive surface water coverage. Ongoing research initiatives will emphasize the refinement of these model parameterizations and the optimization of spatial interpolation techniques, with a particular focus on enhancing performance during extreme events.

2.2.2 CYGNSS Data

In this study, we use the Delay Doppler Map (DDM) signal-to-noise ratio (SNR) of the level 1, version 3.1 CYGNSS data, which is publicly accessible through the Physical Oceanography Distributed Active Archive Center (https://podaac.jpl.nasa.gov/CYGNSS) to produce a surface reflectivity (SR) signal based on the methodology in (Gerlein-Safdi & Ruf, 2019). The SNR was corrected for receiving and transmitting antenna gains, transmitted power level, and propagation loss from transmitter to specular point and specular point to receiver, assuming coherent scattering as described in (C. Chew et al., 2018):

$$\mathrm{SR}^{\mathrm{coherent}} = \mathrm{SNR} - P_r^t - G^r - G^t + 20\log_{10}(\lambda) + 20\log_{10}(\mathrm{TxSP} + \mathrm{SPRx}) + 20\log_{10}(4\pi) \quad (1)$$

where P_{r}^t represents the transmitted power (in dBW), G^r and G^t refer to the receiving and transmitter antenna gains (in dB), respectively, λ denotes the GPS wavelength, which is equal to 0.19 m, the distances between the transmitter and the specular point, and between the specular point and the receiver, are denoted by TxSP and SPRx, respectively (both in meters). To provide a comparable range of variation in SR data to the initial SNR range, we removed the average of the 5% lowest data, which is a method employed in previous studies (C. Chew et al., 2018; Gerlein-Safdi & Ruf, 2019; Gerlein-Safdi et al., 2021).

The available CYGNSS data at the time of investigation, covering from August 2018 to September 2023, was processed in this study. It is noteworthy that the time coverage of level 1, version 3.1 CYGNSS data begins in August 2018, in contrast to the earlier level 1, version 2.1 data used in previous studies (Gerlein-Safdi & Ruf, 2019; Gerlein-Safdi et al., 2021), which starts from June 2017. Prior to August 1, 2018, the CYGNSS data was obtained using the GPS navigation receiver's automatic gain control (AGC) mode, which restricted the strength of direct signals received from GPS satellites to a narrow dynamic range before signal processing. The AGC mode was disabled to allow the use of direct signal strength to monitor GPS transmit power level and improve calibration (C. Ruf, 2022), and resulted in a change in the time span for L1 and higher data products from the Sensor Data Record (SDR) version 3.0 onward.

3 Methodology

The methodology initially developed by Gerlein-Safdi et al.(Gerlein-Safdi & Ruf, 2019; Gerlein-Safdi et al., 2021) for generating watermasks leverages both the spatial and temporal information contained in the SR data, and applies the random walker algorithm from the Python scikit-image library (https://scikit-image.org/) (van der Walt et al., 2014) to segment water and land. This approach does not rely heavily on data aggregation and is particularly well-suited for studying hydrological processes that exhibit seasonal variations. Here we present an extension of this exploratory work, which involves the establishment of a robust parameter and threshold selection system that can be applied regardless of the domain, as well as the coupling of surface topography data with the computer vision algorithm to optimize image segmentation with spatial analysis. By utilizing this methodology, we successfully generated a CYGNSS-based monthly watermasks product with a grid size of $0.01^\circ \times 0.01^\circ$(∼1 km×1 km) and covers a latitudinal range from 37.4°N to 37.4°S. This product represents a continuous timeline spanning from August 2018 to the present and will be updated on a monthly basis.

3.1 Pre-Labeling

The random walk approach proposed by Grady in (Grady, 2016) performs multilabel, interactive image segmentation. The method requires a set of pre-labeled pixels (seed points), which we refer to as markers throughout this work. The algorithm functions by labeling unseeded pixels with the respective label of the seed point that a random walker, with a bias to avoid crossing object boundaries (i.e., intensity gradients), is expected to reach first when initiated from that pixel. The calculation can be performed analytically (Grady, 2016), leading to an efficient and precise image segmentation. In the prior investigation (Gerlein-Safdi et al., 2021), markers were allocated based on both monthly SR and the number of standard deviations(STD) from yearly average, which was found to be efficient in studying domains that exhibit high seasonal variations. In order to ensure that water bodies with low seasonal variations are also being captured as we are extending the study towards the entire CYGNSS domain, we propose a combination of four parameters for pre-labeling pixel: SR, STD, SW, and ACC as further explained below.

3.1.1 SR Map

For each month, the *SR Map* is generated by gridding monthly SR values into a $0.01^\circ \times 0.01^\circ$ grid. Each grid cell contains the entire distribution of CYGNSS overpasses that occurred within its bounds. In cases where a grid cell contains more than one SR data, the monthly SR pixel is assigned with the average of the SR values. We then use a nearest neighbor interpolation method (SciPy, https://scipy.org/) to populate missing data for any pixels.

3.1.2 STD Map

The *STD Map* is produced by assessing the deviation of SR value for each individual pixel from its 5-year average, using the yearly average and STD values. The computed STD map shows the number of STDs from the yearly average, and as such, a negative value signifies drier-than-usual conditions for that month, while a positive value indicates wetter-than-usual conditions for the corresponding pixel.

3.1.3 SW Map

The static water *SW Map* is produced by taking the 5^{th} percentile value in the yearly SR distribution for each pixel. Static water bodies can be effectively discerned using this strategy, as their SR value distribution is typically highly concentrated at elevated levels, which are evident as the 5^{th} percentile value. Figure 1 provides an illustrative example of the notable contrast between the surface reflectivity distributions for always dry and always wet pixels using a violin plot.

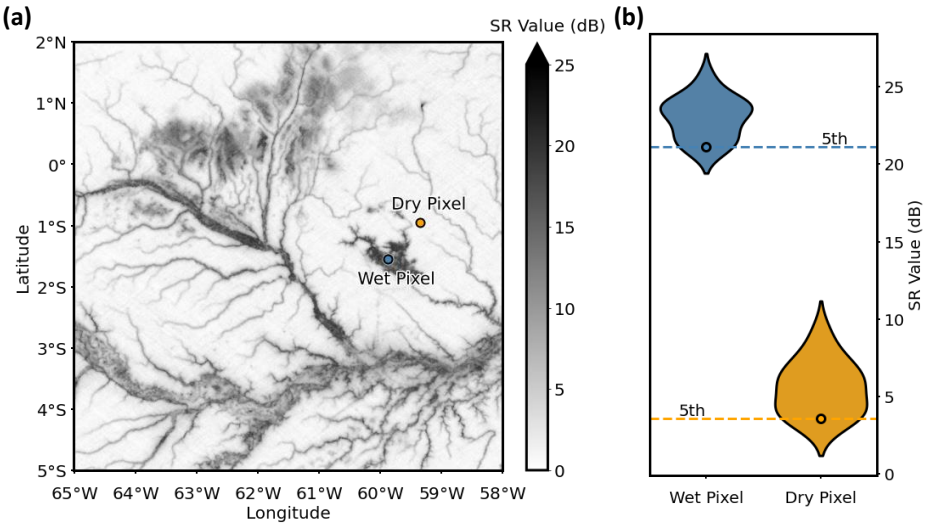

Figure 1: An illustration of long-term dry and wet pixels. (a) Long-term dry areas (in orange) and wet areas (in blue) are shown on the static water (SW) map, which consists of the 5^{th} percentile value in the yearly SR distribution for each pixel. (b) The yearly SR value distribution for the two pixels respectively. Their 5^{th} percentile values (SW) are marked with dash lines.

3.1.4 ACC Map

The *ACC Map* uses flow accumulation, which is a geospatial product that is obtained by processing a digital elevation model (DEM). The calculation involves assigning a value to each pixel that corresponds to the number of upstream pixels that flow into it. This value is referred to as the accumulated grid cell count. We adopted the HydroSHEDS ACC map from (Lehner et al., 2008) and the map was re-scaled to ensure its alignment with the grid settings in this study.

3.1.5 Marker Selection

The set of parameters governing the marker allocation process and their respective physical implications are explained in Table 1. If a pixel falls into any category, it will be assigned as a land/water marker. Utilizing part of the Amazon Basin in May 2021 as a rep-

resentative case, Figure 2 elucidates the process of segmentation. The input image, assigned markers, and the resulting segmentation are showcased in Figure 2(a). Additionally, Figure 2(b) provides insights into each individual parameter, displaying their density distributions and exemplifying both upper and lower boundaries.

Table 1: Combining Parameters for Establishing Markers

No.	Parameters	Lower Bound Indication	Upper Bound Indication
1	SR ∩ STD	Dry ∩ Drier than Usual	Wet ∩ Wetter than Usual
2	SR ∩ SW	Dry ∩ Always Dry	Wet ∩ Always Wet
3	SR ∩ ACC	Dry ∩ Drain If Water Exists	Wet ∩ Sink If Water Exists
4	STD ∩ SW	Drier than Usual ∩ Always Dry	Wetter than Usual ∩ Always Wet

3.2 Random Walk with Spatial Analysis

Finally, within the framework of the random walk algorithm, we introduce a new variable termed the "Flow Accumulation Index" (F). It serves to interconnect spatial analysis with the random walk concept. Comprehensive insights into the algorithm's fundamental components are illustrated in (Grady, 2016), regarding graph weight generation, equation establishment for problem-solving, and implementation details. In summary, a graph is defined as $G = (V, E)$, where V represents vertices and E represents edges. In a weighted graph, each edge is assigned a value (weight), denoted as w_{ij}, and the vertex degree d_i is given by $d_i = \sum w_{ij}$ for all incident edges e_{ij}. To interpret w_{ij} as a bias for a random walker choice, it's necessary to set $w_{ij} > 0$. Additionally, an assumption is made for the graph to be connected and undirected (i.e., $w_{ij} = w_{ji}$). The weighting function for calculating edge weight was given by (Grady, 2016):

$$w_{ij} = \exp\left[-\beta \left(g_i - g_j\right)^2\right] \tag{2}$$

where g_i denotes the image intensity at pixel i, and β is the only free parameter in this algorithm. As pointed out in (Grady, 2016), the weight function (2) has the potential to be adapted for use with consideration of features present within an image, such as texture information, filter coefficients, etc. For this study, we modified the weighting function by adding the Flow Accumulation Index (F): the updated weighting function then becomes:

$$w_{ij} = \exp\left[-\beta \left(g_i F_i - g_j F_j\right)^2\right] \tag{3}$$

where F is a re-weighted index based on the flow accumulation (ACC). The result provides adjustments to the segmentation results, where individual pools are linked if that is what the topography favors, and vice versa as Figure 3(a) shows. Figure 3(b) provides corresponding references to the Digital Elevation Model (DEM) map and Accumulated Flow Accumulation (ACC) map.

3.3 Mitigate False Positives and False Negatives

To improve the precision of the algorithm as it is scaled up to a broader spatial domain, we have meticulously addressed instances of both false negatives and false positives within the workflow. This strategic approach ensures a more accurate and reliable application of the algorithm across diverse scenarios.

To enhance dataset integrity, we implemented a filtering step to remove any pixel exhibiting anomalously high or low SR values compared to adjacent months. This process effectively addresses outliers when assigning markers.

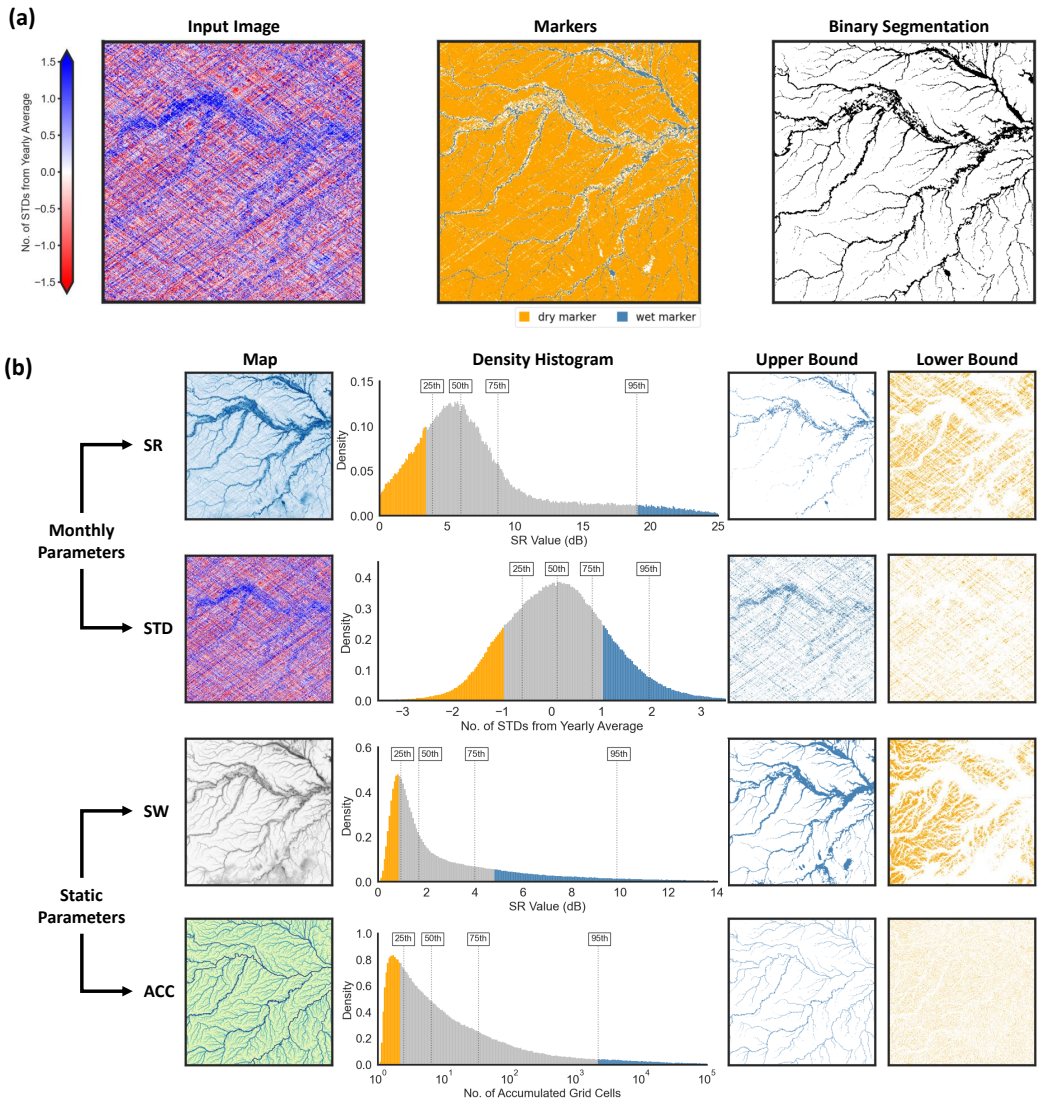

Figure 2: Illustration of the image segmentation process. (a) Left: Input image subjected to segmentation, known as the Monthly STD Map. Center: Allocated markers. Right: Resulting segmentation. (b) Individual parameters featuring their density distribution, along with instances of upper and lower bounds.

In addition, the Unsharp Mask (USM) technique, explained in (Gonzalez & Woods, 2018), is employed to increase contrast along object edges in the image, effectively identifies pixels whose values significantly differ from their neighboring pixels, meanwhile it does not explicitly detect edges. The method serves as a critical reference tool in marker assignment, particularly in ensuring the quality of markers in areas and in periods that are characterized by high moisture backgrounds. It significantly improves the accuracy of marker placement by highlighting subtle contrasts and details in moisture-rich environments.

Moreover, dry and flat regions, such as flat deserts, pose challenges as potential false positives due to their high SR values (Carreno-Luengo et al., 2019; Hodges et al., 2023). We flagged out the dry and flat regions when assigning markers through cross-referencing the World Terrestrial Ecosystem (WTE) 2020 database (Sayre, 2022) in conjunction with a slope

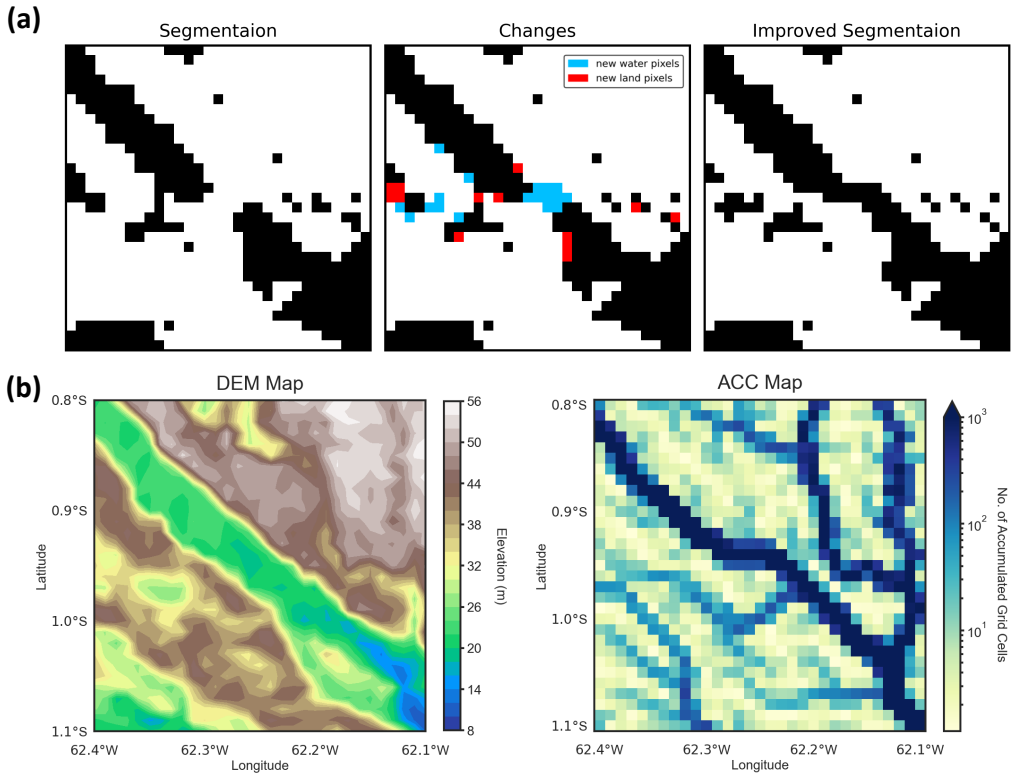

Figure 3: (a) Illustration of the adjustments made to improve segmentation results, where individual pools are connected or separated based on topographical features. (b) Corresponding Digital Elevation Model (DEM) map and Accumulated Flow Accumulation (ACC) map.

map derived from the HydroSHEDS DEM (Lehner et al., 2008). Specifically, pixels were systematically excluded from the water marker category if they satisfied the upper bound criteria 2-4 in Table 1, while concurrently being classified in WTE as *Plains* or *Tablelands* in the Landform Class, *Dry* or *Desert* in the Moisture Class, and *Settlement*, *Shrubland*, or *Sparsely or Non-vegetated* in the Landcover Class and additionally exhibiting a slope of less than 0.05° in the DEM data.

Further, the presence of wind-induced surface roughness in large open water areas can lead to low SR values, resulting in portions of large open water domains being unaccounted for by the algorithm. This phenomenon is exemplified by Lake Victoria in Africa. To mitigate these uncertainties and effectively address the missing data in large water bodies, we apply a layer of data that identifies regions where water occurrence exceeds 95% based on the Global Surface Water Explorer(GSWE)(Pekel et al., 2016).

Lastly, regions surpassing the DDM height limit of 4100 meters are recognized to have insufficient data availability. Pixels exceeding this altitude threshold are marked as null, reducing the likelihood of overlooking significant water bodies and therefore avoiding false negatives in high-altitude areas.

This workflow addresses various geographical and environmental factors and aids in refining the algorithm with diverse landscapes.

3.4 Tilling

The CYGNSS domain is partitioned into tiles of size 10° × 10°, and the algorithm is applied to each tile. More details regarding the tiling are described in the supporting information (Figure S1). Notably, the algorithm exhibited robustness in that the parameters were established based on the distribution within each tile, and the markers could be assigned without impacting the resulting water mask. Besides, the dynamic threshold is a crucial component of the algorithm because it ensures consistent performance across various regions and different time frames. In different geographical areas, vegetation can undergo significant changes, making it essential for the algorithm to adapt and maintain its accuracy. By adjusting its thresholds dynamically, the algorithm can effectively address these variations and deliver reliable results regardless of the specific location or time period it is applied to. Figure 4 shows how the Amazon region becomes segmented into four tiles and serves as a demonstration of the algorithm's robustness, as the markers are not assigned uniformly, yet the resulting water mask remains unaffected by the tile boundaries.

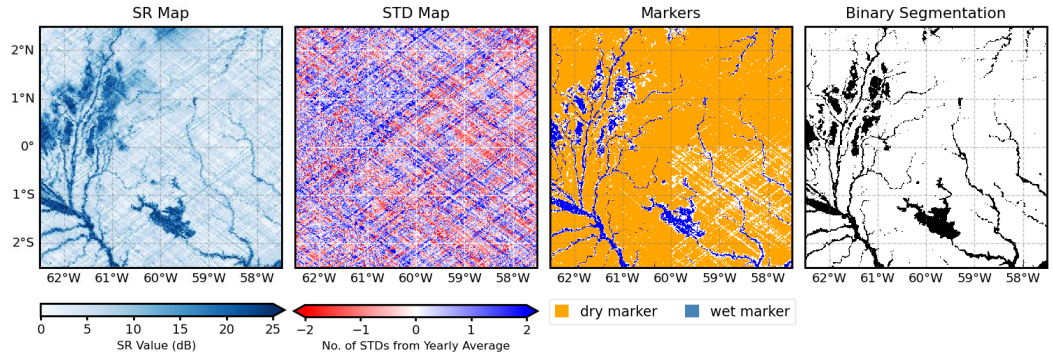

Figure 4: Illustration of the CYGNSS algorithm's robustness in tiling. Far-left: SR Map. Center-left: STD Map. Center-right: non-uniform marker assignments aligned with the tiles. Far-right: the resulting water mask, which remains unaffected by non-uniform marker assignments.

4 Results

Figure 5 presents May 2023 as an example of the watermask. Many large wetland and river basins are easily identifiable, even when zoomed out, including the Amazon Basin, the Pantanal, the Congo Basin, the Sudd, or the Yangtze River. Note the greyed areas over the Himalayas and the Andes, indicating areas of elevation higher than 4100 m over which the algorithm was not applied (see Section 3.3). An animation of the full timeseries from August 2018 to September 2023 is available as supplementary information (Movie S1, available online). Strong seasonality shows across the world, with various regions experiencing wet and dry seasons at various points in the year.

4.1 Comparison with SWAMPS and WAD2M

In Figure 6, we showcase regional comparisons that utilize the inundated area fraction (f_w) observed using the Berkeley-RWAWC, SWAMP, and WAD2M data sources between August 2018, when Berkeley-RWAWC product begins, and December 2020, after which date WAD2M and SWAMPS are not available. Berkeley-RWAWC, originally gridded at a spatial resolution of 0.01° (approximately 1 kilometer at the equator), has been downscaled into a resolution of 0.25° for direct comparison. We selected four geographically diverse regions - namely the Amazon Basin, the Pantanal, the Sudd, and the Indo-Gangetic Plain - each representing distinct ecological and geographical contexts. Figure 6 indicates that the CYGNSS product exhibits a remarkable capacity to elucidate pronounced seasonal vari-

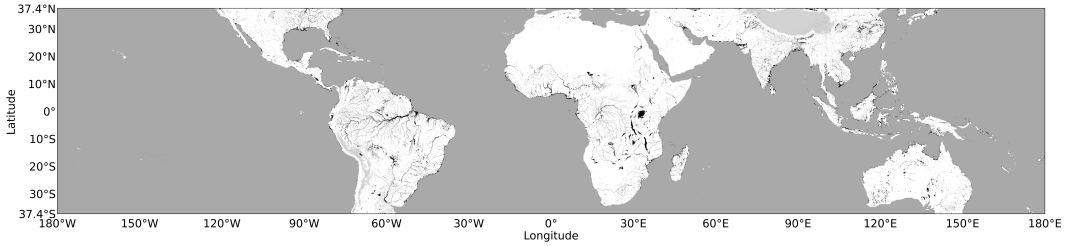

Figure 5: The Berkeley-RWAWC water extent map for May 2023. Inland water is shown in black, dry land in white, and grey areas depict either oceans or areas of high elevation where not enough data is available to produce accurate maps (e.g. the Himalayas and the Andes).

ations in surface water dynamics compared to the other two datasets. Furthermore, we present the monthly maps for the year 2020 for these four distinct geographical regions as captured by the three datasets, accessible in Supporting Information Figure S2.

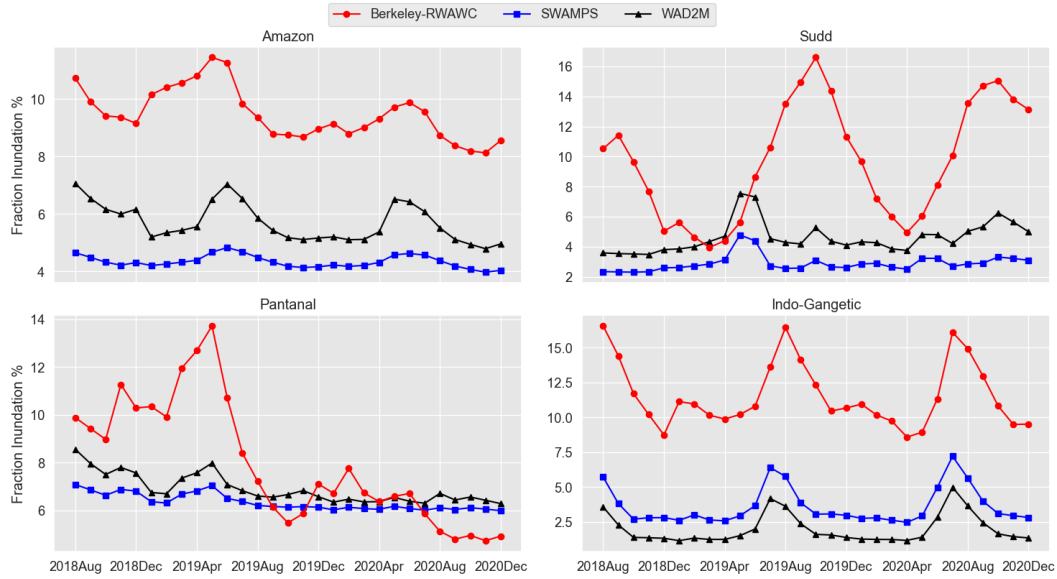

Figure 6: Regional comparisons of the timeseries of the inundated area fraction (f_w) observed for Berkeley-RWAWC (red), SWAMP (blue), and WAD2M (black) products between August 2018 and December 2020 over the Amazon Basin (upper left), the Sudd wetland (upper right), the Pantanal wetland (lower left), and the Indo-Gangetic Plain (lower right).

It is interesting to note that WAD2M, which is supposed to be an improved version of the SWAMPS product, shows a higher extent than SWAMPS in three of the four locations, the Indo-Gangetic Plain being the exception. The Berkeley-RWAWC results for the Amazon and the Indo-Gangetic Plain exhibit similar seasonal patterns when compared to SWAMP and WAD2M datasets. However, it is noteworthy that the mean average within the CYGNSS dataset is significantly higher than that observed in the other two datasets. For the Sudd, Berkeley-RWAWC data presents more pronounced and dramatic seasonal variations compared to SWAMP and WAD2M datasets. In addition, we see an offset in the seasonality of the three products, with SWAMP and the WAD2M peaking in late spring for just three months (e.g. April, May, and June of 2019) and staying stable otherwise, whereas Berkeley-RWAWC shows instead a pronounced seasonal pattern and reaches its maximal

extent in late summer, with peaking evident in September and October. In the case of the Pantanal region, the Berkeley-RWAWC maps reveal a distinct high water extent peak in May 2019, a feature absent in the SWAMP and WAD2M datasets. Figure 7 shows the inundation fraction in the Berkeley-RWAWC product over the Sudd and the Pantanal for an extended time window going until 2023 September. Broader trends emerge then: over the 5 years of data, the Sudd shows a regular seasonal range but exhibits a strong inter-annual upward trend. The Pantanal on the other hand shows a large interannual variability, with 2019 and 2023 showing large inundation extent, whereas 2020, 2021, and 2022 show much smaller peak wet season extent. No long-term trend is appearing in the Pantanal.

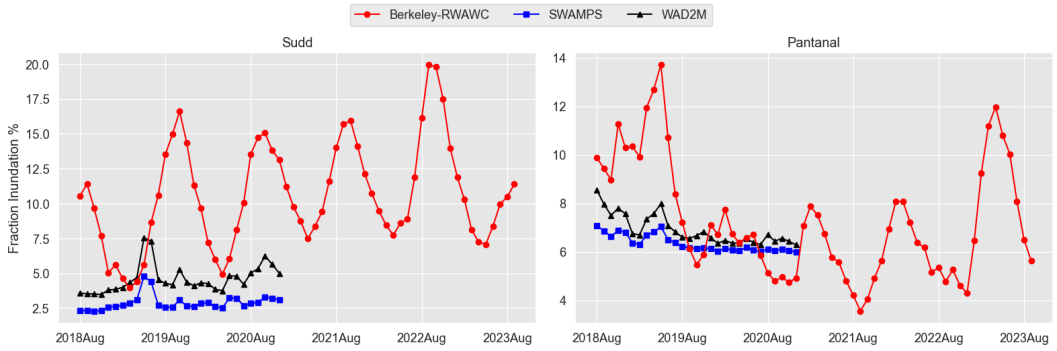

Figure 7: Regional comparisons of the inundated area fraction (f_w) observed for Berkeley-RWAWC (red), SWAMP (blue), and WAD2M (black) over the Sudd (left) and the Pantanal (right). Here, Berkeley RWAWC is shown until September 2023. WAD2M and SWAMPS end in December 2020 after which date the two datasets are not available.

5 Discussion

The new Berkeley-RWAWC product is a unique tool to understand the spatio-temporal dynamics of inland waterbodies in the Tropics and sub-Tropics. Being updated in near-real time, the product will allow for rapid estimation of seasonal patterns as they emerge. The product exhibits a much higher seasonal variability than WAD2M and SWAMPS, two products regularly used to capture inland waterbodies (Xi et al., 2023; Liu & Zhuang, 2023; Deng et al., 2022; Skeie et al., 2023; Z. Zhang et al., 2023). This heightened sensitivity to seasonal variability carries profound implications across an array of scientific disciplines. The capacity to discern more changes in surface water dynamics opens up a plethora of opportunities for the scientific community to advance our understanding of critical ecological processes and environmental management.

The product's advanced monitoring capabilities offer a valuable tool in the fight against climate change, helping to identify and manage one of the key sources of greenhouse gas emissions. Wetlands are known to be substantial sources of methane, a potent greenhouse gas, and understanding their dynamics is crucial for climate change mitigation efforts. By providing detailed insights into the timing and duration of wetland inundation, the product enables researchers to pinpoint when and where methane emissions are most likely to occur. This information is essential for developing targeted strategies to better understand and predict methane release from wetlands in a changing climate. Additionally, the product's ability to track changes in wetland conditions over time allows for the assessment of how different environmental factors, including human interventions, affect methane emission rates. This could be particularly beneficial in identifying areas where methane emissions are increasing and require urgent attention. The Berkeley-RWAWC product has already been leveraged for this purpose in multiple studies (Gerlein-Safdi et al., 2021; Lin et al., 2023), with more ongoing efforts leveraging the product currently in the work. For example, the implications of the increasing trend in inundation observed over the Sudd by the Berkeley-

RWAWC might help explain the large, ever-growing methane emission signal being detected by methane monitoring satellites over the area (Frankenberg et al., 2011; Hu et al., 2018; Lunt et al., 2019).

Another pivotal application lies in unraveling the intricate interplay between fire regimes and wetland refilling patterns (Martin, 2016; Williams-Jara et al., 2022; Kominoski et al., 2022). The product can provide crucial insights into the timing and duration of inundation events, enabling researchers to assess how wetland refill rates may influence fire frequency, intensity, and ecological resilience, or the other way around. This knowledge is indispensable for fire management strategies and the conservation of vulnerable wetland ecosystems. Furthermore, the enhanced ability to monitor seasonal variations in wetlands has direct implications for wetland conservation efforts. For example, the high inundation wet season in 2018/2019 followed by low water years in 2019/2020 observed in the Pantanal might be associated with the catastrophic fire event that engulfed the Pantanal wetlands in both 2019 and 2020 (Leal Filho et al., 2021). The aftermath of this extensive fire outbreak raises concerns regarding the long-term ecological consequences, as initial indications suggest that the Pantanal's unique biodiversity hotspot may face challenges in fully recovering from the unprecedented scale of these fires (Marques et al., 2021; Correa et al., 2022).

Additionally, inland waterbodies serve as vital habitats for diverse flora and fauna, playing an essential role in maintaining biodiversity (Zedler & Kercher, 2005). With this product, researchers can gain a new perspective on wetland dynamics, allowing for a more comprehensive evaluation of conservation strategies. This data can inform the identification of critical wetland areas, guide habitat restoration initiatives, and facilitate sustainable land use planning to safeguard these invaluable ecosystems. For example, in the realm of biodiversity conservation, this product offers an advantage in tracking the movements of wildlife that traverse multiple wetlands throughout the year. Many species, such as migration birds and amphibians, rely on wetlands as stopover points during their journeys (Somveille et al., 2013; Runge et al., 2015). By providing a clearer view of wetland dynamics, the product aids in understanding the availability and accessibility of suitable habitats for these nomadic species. Researchers can use this information to devise effective conservation strategies that ensure the continuity of vital habitats, contributing to the preservation of biodiversity on a global scale.

Finally, this new product, with its high sensitivity to seasonal variations in inland waterbodies, not only wetlands but also rivers, might be a great tool to test theories related to river networks, their formations, and their sequential activation (Rinaldo et al., 2014; Bertassello et al., 2022; Durighetto et al., 2023). The tools being developed to better understand river networks are of crucial importance to understanding the hydrological response of river basins to extreme hydrological events, but data to appropriately test these theories have so far been very limited, both spatially and temporally.

In sum, the product's capacity to illuminate seasonal variability in surface water dynamics holds transformative potential for a myriad of scientific applications. From fire ecology and wetland conservation to biodiversity preservation and to methane emission, the data generated by the product enriches our ability to comprehend and address complex environmental challenges, fostering a more informed and proactive approach to safeguarding our planet's ecosystems and natural resources. While the product exhibits enhanced performance in capturing seasonal variations, it is crucial to acknowledge its inherent nature as a binary water mask. With a resolution of 0.01° in both latitude and longitude, each pixel stands as a definitive sentinel, representing either a watery domain or dry land within a compact ∼1km by 1km frame. This singular feature underscores the need for users to embrace the binary essence of our data product, acknowledging its precision level and distinctiveness when harnessing it for diverse applications.

6 Conclusions

This article presented the Berkeley-RWAWC inundation product, addressing a critical research gap in global inland water dynamics. Historically, challenges like cloud cover, dense vegetation, and limited remote sensing revisit frequency hindered the characterization of seasonal inundation in tropical regions. Our study presents a significant advancement by adapting a computer vision algorithm for CYGNSS-based inundation mapping. Applied since August 2018, it enables monthly mapping at a 0.01° spatial resolution ($\sim$ 1km). We detail our workflow and parameterization strategy. This methodology distinguishes itself by exclusively relying on static products combined with CYGNSS data for product development. This deliberate choice provides our results with a robust indication of CYGNSS data's unique contributions, setting our dataset apart from others in the field. Comparative analysis with SWAMPS and WAD2M in the Amazon, the Pantanal, the Sudd, and the Indo-Gangetic plain reveals higher seasonal variations in Berkeley-RWAWC. We discuss Berkeley-RWAWC's applications, emphasizing its role in advancing tropical hydrology. To enhance access, we introduce a data portal for the scientific community. This paper contributes to remote sensing and hydrology knowledge, improving insights into tropical wetland dynamics and their global hydrological significance.

7 Data Availability

The monthly netCDF files for the Berkeley-RWAWC product over the entire CYGNSS domain are available via Globus at the following URL: `https://shorturl.at/bdr46`. The data is also available for visualization on the NASA VEDA dashboard: `http://tinyurl.com/mt3m78zy`. The WAD2M data is available for download as a netCDF file from Zenodo (doi: 10.5281/zenodo.3998453) (Z. Zhang et al., 2021a). The SWAMPS v3.2 dataset is downloadable from the Alaska Satellite Facility DAAC at the following url: `https://asf.alaska.edu/data-sets/derived-data-sets/wetlands-measures/wetlands-measures-product-downloads/#swamps`. The CYGNSS data, L1 v3.1 used in this study is available from the PO.DAAC (`https://podaac.jpl.nasa.gov/dataset/CYGNSS_L1_V3.1`) (CYGNSS, 2021).

Acknowledgments
All authors are supported by the National Aeronautics and Space Administration under Grant No. 80NSSC21K1005.

References

Al-Khaldi, M. M., Johnson, J. T., O'Brien, A. J., Balenzano, A., & Mattia, F. (2019, July). Time-Series Retrieval of Soil Moisture Using CYGNSS. *IEEE Transactions on Geoscience and Remote Sensing*, *57*(7), 4322–4331. Retrieved 2023-10-30, from `https://ieeexplore.ieee.org/document/8631126` (Conference Name: IEEE Transactions on Geoscience and Remote Sensing) doi: 10.1109/TGRS.2018.2890646

Al-Khaldi, M. M., Shah, R., Chew, C. C., Johnson, J. T., & Gleason, S. (2021). Mapping the Dynamics of the South Asian Monsoon Using CYGNSS's Level-1 Signal Coherency. *IEEE Journal of Selected Topics in Applied Earth Observations and Remote Sensing*, *14*, 1111–1119. Retrieved 2023-10-30, from `https://ieeexplore.ieee.org/document/9280328` (Conference Name: IEEE Journal of Selected Topics in Applied Earth Observations and Remote Sensing) doi: 10.1109/JSTARS.2020.3042170

Alsdorf, D. E., Rodríguez, E., & Lettenmaier, D. P. (2007). Measuring surface water from space. *Reviews of Geophysics*, *45*(2). Retrieved 2023-10-30, from `https://onlinelibrary.wiley.com/doi/abs/10.1029/2006RG000197` (_eprint: https://onlinelibrary.wiley.com/doi/pdf/10.1029/2006RG000197) doi: 10.1029/2006RG000197

Bertassello, L. E., Durighetto, N., & Botter, G. (2022, November). Eco-hydrological

modelling of channel network dynamics—part 2: application to metapopulation dynamics. *Royal Society Open Science*, *9*(11), 220945. Retrieved 2023-12-20, from https://royalsocietypublishing.org/doi/10.1098/rsos.220945 doi: 10.1098/rsos.220945

Betts, R. A., Alfieri, L., Bradshaw, C., Caesar, J., Feyen, L., Friedlingstein, P., ... Wyser, K. (2018, April). Changes in climate extremes, fresh water availability and vulnerability to food insecurity projected at 1.5°C and 2°C global warming with a higher-resolution global climate model. *Philosophical Transactions of the Royal Society A: Mathematical, Physical and Engineering Sciences*, *376*(2119), 20160452. Retrieved 2023-10-26, from https://royalsocietypublishing.org/doi/full/10.1098/rsta.2016.0452 (Publisher: Royal Society) doi: 10.1098/rsta.2016.0452

Bloom, A. A., Bowman, K. W., Lee, M., Turner, A. J., Schroeder, R., Worden, J. R., ... Jacob, D. J. (2017, June). A global wetland methane emissions and uncertainty dataset for atmospheric chemical transport models (WetCHARTs version 1.0). *Geoscientific Model Development*, *10*(6), 2141–2156. Retrieved 2023-09-26, from https://gmd.copernicus.org/articles/10/2141/2017/ (Publisher: Copernicus GmbH) doi: 10.5194/gmd-10-2141-2017

Carreno-Luengo, H., Luzi, G., & Crosetto, M. (2019, January). First Evaluation of Topography on GNSS-R: An Empirical Study Based on a Digital Elevation Model. *Remote Sensing*, *11*(21), 2556. Retrieved 2023-12-18, from https://www.mdpi.com/2072-4292/11/21/2556 (Number: 21 Publisher: Multidisciplinary Digital Publishing Institute) doi: 10.3390/rs11212556

Chapman, B. D., Russo, I. M., Galdi, C., Morris, M., di Bisceglie, M., Zuffada, C., ... O'Brien, A. J. (2022). Comparison of SAR and CYGNSS Surface Water Extent Metrics. *IEEE Journal of Selected Topics in Applied Earth Observations and Remote Sensing*, *15*, 3235–3245. Retrieved 2023-10-25, from https://ieeexplore.ieee.org/document/9745185 (Conference Name: IEEE Journal of Selected Topics in Applied Earth Observations and Remote Sensing) doi: 10.1109/JSTARS.2022.3162764

Chew, C., Reager, J. T., & Small, E. (2018). CYGNSS data map flood inundation during the 2017 atlantic hurricane season. *Scientific Reports*, *8*(1), 9336. Retrieved 2023-03-14, from https://www.nature.com/articles/s41598-018-27673-x (Number: 1 Publisher: Nature Publishing Group) doi: 10.1038/s41598-018-27673-x

Chew, C., Small, E., & Huelsing, H. (2023, August). Flooding and inundation maps using interpolated CYGNSS reflectivity observations. *Remote Sensing of Environment*, *293*, 113598. Retrieved 2023-10-25, from https://www.sciencedirect.com/science/article/pii/S0034425723001499 doi: 10.1016/j.rse.2023.113598

Chew, C. C., & Small, E. E. (2018). Soil moisture sensing using spaceborne GNSS reflections: Comparison of CYGNSS reflectivity to SMAP soil moisture. *Geophysical Research Letters*, *45*(9), 4049–4057. Retrieved 2023-03-14, from https://onlinelibrary.wiley.com/doi/abs/10.1029/2018GL077905 (_eprint: https://onlinelibrary.wiley.com/doi/pdf/10.1029/2018GL077905) doi: 10.1029/2018GL077905

Clarizia, M. P., Pierdicca, N., Costantini, F., & Floury, N. (2019, July). Analysis of CYGNSS Data for Soil Moisture Retrieval. *IEEE Journal of Selected Topics in Applied Earth Observations and Remote Sensing*, *12*(7), 2227–2235. Retrieved 2023-10-30, from https://ieeexplore.ieee.org/document/8645800 (Conference Name: IEEE Journal of Selected Topics in Applied Earth Observations and Remote Sensing) doi: 10.1109/JSTARS.2019.2895510

Correa, D. B., Alcântara, E., Libonati, R., Massi, K. G., & Park, E. (2022, August). Increased burned area in the Pantanal over the past two decades. *Science of The Total Environment*, *835*, 155386. Retrieved 2023-12-31, from https://www.sciencedirect.com/science/article/pii/S0048969722024792 doi: 10.1016/j.scitotenv.2022.155386

CYGNSS. (2021). *Cygnss level 1 science data record version 3.1.* NASA Physical Oceanography Distributed Active Archive Center. Retrieved from https://podaac.jpl.nasa

.gov/dataset/CYGNSS_L1_V3.1 doi: 10.5067/CYGNS-L1X31

Das Gupta, M. (2014, February). Population, Poverty, and Climate Change. *The World Bank Research Observer*, *29*(1), 83–108. Retrieved 2023-10-26, from https://doi.org/10.1093/wbro/lkt009 doi: 10.1093/wbro/lkt009

Deng, Z., Ciais, P., Tzompa-Sosa, Z. A., Saunois, M., Qiu, C., Tan, C., ... Chevallier, F. (2022). Comparing national greenhouse gas budgets reported in unfccc inventories against atmospheric inversions. *Earth System Science Data*, *14*(4), 1639–1675. Retrieved from https://essd.copernicus.org/articles/14/1639/2022/ doi: 10.5194/essd-14-1639-2022

Dong, F., Wang, Y., Su, B., Hua, Y., & Zhang, Y. (2019, February). The process of peak CO2 emissions in developed economies: A perspective of industrialization and urbanization. *Resources, Conservation and Recycling*, *141*, 61–75. Retrieved 2023-10-26, from https://www.sciencedirect.com/science/article/pii/S0921344918303756 doi: 10.1016/j.resconrec.2018.10.010

Downs, B., Kettner, A. J., Chapman, B. D., Brakenridge, G. R., O'Brien, A. J., & Zuffada, C. (2023). Assessing the Relative Performance of GNSS-R Flood Extent Observations: Case Study in South Sudan. *IEEE Transactions on Geoscience and Remote Sensing*, *61*, 1–13. Retrieved 2023-10-30, from https://ieeexplore.ieee.org/document/10018248 (Conference Name: IEEE Transactions on Geoscience and Remote Sensing) doi: 10.1109/TGRS.2023.3237461

Durighetto, N., Noto, S., Tauro, F., Grimaldi, S., & Botter, G. (2023). Integrating spatially- and temporally-heterogeneous data on river network dynamics using graph theory. *iScience*, *26*(8), 107417. Retrieved from https://www.sciencedirect.com/science/article/pii/S2589004223014943 doi: https://doi.org/10.1016/j.isci.2023.107417

Entekhabi, D., Njoku, E. G., O'Neill, P. E., Kellogg, K. H., Crow, W. T., Edelstein, W. N., ... Van Zyl, J. (2010, May). The Soil Moisture Active Passive (SMAP) Mission. *Proceedings of the IEEE*, *98*(5), 704–716. Retrieved 2023-10-25, from http://ieeexplore.ieee.org/document/5460980/ doi: 10.1109/JPROC.2010.2043918

Eroglu, O., Kurum, M., Boyd, D., & Gurbuz, A. C. (2019, January). High Spatio-Temporal Resolution CYGNSS Soil Moisture Estimates Using Artificial Neural Networks. *Remote Sensing*, *11*(19), 2272. Retrieved 2023-10-30, from https://www.mdpi.com/2072-4292/11/19/2272 (Number: 19 Publisher: Multidisciplinary Digital Publishing Institute) doi: 10.3390/rs11192272

Fekete, B. M., Vörösmarty, C. J., & Grabs, W. (2002). High-resolution fields of global runoff combining observed river discharge and simulated water balances. *Global Biogeochemical Cycles*, *16*(3), 15–1–15–10. Retrieved 2023-10-23, from https://onlinelibrary.wiley.com/doi/abs/10.1029/1999GB001254 (_eprint: https://onlinelibrary.wiley.com/doi/pdf/10.1029/1999GB001254) doi: 10.1029/1999GB001254

Finlayson, C. M., & Spiers, A. G. (Eds.). (1999). *Global review of wetland resources and priorities for wetland inventory* (No. 144). Canberra: Supervising Scientist.

Frankenberg, C., Aben, I., Bergamaschi, P., Dlugokencky, E. J., van Hees, R., Houweling, S., ... Tol, P. (2011). Global column-averaged methane mixing ratios from 2003 to 2009 as derived from sciamachy: Trends and variability. *Journal of Geophysical Research: Atmospheres*, *116*(D4). Retrieved from https://agupubs.onlinelibrary.wiley.com/doi/abs/10.1029/2010JD014849 doi: https://doi.org/10.1029/2010JD014849

Gerlein-Safdi, C., Bloom, A. A., Plant, G., Kort, E. A., & Ruf, C. S. (2021). Improving representation of tropical wetland methane emissions with CYGNSS inundation maps. *Global Biogeochemical Cycles*, *35*(12), e2020GB006890. Retrieved 2023-03-14, from https://onlinelibrary.wiley.com/doi/abs/10.1029/2020GB006890 doi: 10.1029/2020GB006890

Gerlein-Safdi, C., & Ruf, C. S. (2019). A CYGNSS-Based Algorithm for the Detection of Inland Waterbodies. *Geophysical Research Letters*, *46*(21), 12065–12072. Retrieved 2023-03-14, from https://onlinelibrary.wiley.com/doi/abs/10.1029/2019GL085134 (_eprint:

https://onlinelibrary.wiley.com/doi/pdf/10.1029/2019GL085134) doi: 10.1029/2019GL085134

Gleason, S., Hodgart, S., Yiping Sun, Gommenginger, C., Mackin, S., Adjrad, M., & Unwin, M. (2005, June). Detection and Processing of bistatically reflected GPS signals from low Earth orbit for the purpose of ocean remote sensing. *IEEE Transactions on Geoscience and Remote Sensing*, *43*(6), 1229–1241. Retrieved 2023-09-26, from http://ieeexplore.ieee.org/document/1433022/ doi: 10.1109/TGRS.2005.845643

Gonzalez, R. C., & Woods, R. E. (2018). *Digital image processing.* New York, NY: Pearson.

Grady, L. (2016). Random walks for image segmentation. *IEEE Transactions on Pattern Analysis and Machine Intelligence*, *28*(11), 1768–1783. (Conference Name: IEEE Transactions on Pattern Analysis and Machine Intelligence) doi: 10.1109/TPAMI.2006.233

Hodges, E., Campbell, J. D., Melebari, A., Bringer, A., Johnson, J. T., & Moghaddam, M. (2023). Using Lidar Digital Elevation Models for Reflectometry Land Applications. *IEEE Transactions on Geoscience and Remote Sensing*, *61*, 1–9. Retrieved 2023-12-18, from https://ieeexplore.ieee.org/abstract/document/10066308 (Conference Name: IEEE Transactions on Geoscience and Remote Sensing) doi: 10.1109/TGRS.2023.3256303

Hu, H., Landgraf, J., Detmers, R., Borsdorff, T., Aan de Brugh, J., Aben, I., ... Hasekamp, O. (2018, April). Toward Global Mapping of Methane With TROPOMI: First Results and Intersatellite Comparison to GOSAT. *Geophysical Research Letters*, *45*(8), 3682–3689. Retrieved 2023-03-22, from https://onlinelibrary.wiley.com/doi/abs/10.1002/2018GL077259 doi: 10.1002/2018GL077259

IPCC. (2023, July). *IPCC, 2023: Climate Change 2023: Synthesis Report. Contribution of Working Groups I, II and III to the Sixth Assessment Report of the Intergovernmental Panel on Climate Change [Core Writing Team, H. Lee and J. Romero (eds.)]. IPCC, Geneva, Switzerland.* (Tech. Rep.). Intergovernmental Panel on Climate Change (IPCC). Retrieved 2023-10-26, from https://www.ipcc.ch/report/ar6/syr/ (Edition: First) doi: 10.59327/IPCC/AR6-9789291691647

Jensen, K., & Mcdonald, K. (2019, September). Surface Water Microwave Product Series Version 3: A Near-Real Time and 25-Year Historical Global Inundated Area Fraction Time Series From Active and Passive Microwave Remote Sensing. *IEEE Geoscience and Remote Sensing Letters*, *16*(9), 1402–1406. Retrieved 2023-09-26, from https://ieeexplore.ieee.org/document/8662682/ doi: 10.1109/LGRS.2019.2898779

Justice, C., Townshend, J., Vermote, E., Masuoka, E., Wolfe, R., Saleous, N., ... Morisette, J. (2002, November). An overview of MODIS Land data processing and product status. *Remote Sensing of Environment*, *83*(1-2), 3–15. Retrieved 2023-10-25, from https://linkinghub.elsevier.com/retrieve/pii/S0034425702000846 doi: 10.1016/S0034-4257(02)00084-6

Kellogg, K., Hoffman, P., Standley, S., Shaffer, S., Rosen, P., Edelstein, W., ... Sarma, C. V. H. S. (2020, March). NASA-ISRO Synthetic Aperture Radar (NISAR) Mission. In *2020 IEEE Aerospace Conference* (pp. 1–21). Retrieved 2023-10-27, from https://ieeexplore.ieee.org/abstract/document/9172638 (ISSN: 1095-323X) doi: 10.1109/AERO47225.2020.9172638

Kim, H., & Lakshmi, V. (2018). Use of Cyclone Global Navigation Satellite System (CyGNSS) Observations for Estimation of Soil Moisture. *Geophysical Research Letters*, *45*(16), 8272–8282. Retrieved 2023-10-30, from https://onlinelibrary.wiley.com/doi/abs/10.1029/2018GL078923 (_eprint: https://onlinelibrary.wiley.com/doi/pdf/10.1029/2018GL078923) doi: 10.1029/2018GL078923

Kominoski, J. S., Fernandez, M., Breault, P., Sclater, V., & Rothermel, B. B. (2022, March). Fire Severity and Post-fire Hydrology Drive Nutrient Cycling and Plant Community Recovery in Intermittent Wetlands. *Ecosystems*, *25*(2), 265–278. Retrieved 2023-12-31, from https://doi.org/10.1007/s10021-021-00653-5 doi: 10.1007/s10021-021-00653-5

Konapala, G., Mishra, A. K., Wada, Y., & Mann, M. E. (2020, June). Climate change will affect global water availability through compounding changes in seasonal precipitation and evaporation. *Nature Communications*, *11*(1), 3044. Retrieved 2023-10-23, from https://www.nature.com/articles/s41467-020-16757-w (Number: 1 Publisher: Nature Publishing Group) doi: 10.1038/s41467-020-16757-w

Lange, S., Volkholz, J., Geiger, T., Zhao, F., Vega, I., Veldkamp, T., ... Frieler, K. (2020). Projecting Exposure to Extreme Climate Impact Events Across Six Event Categories and Three Spatial Scales. *Earth's Future*, *8*(12), e2020EF001616. Retrieved 2023-10-26, from https://onlinelibrary.wiley.com/doi/abs/10.1029/2020EF001616 (_eprint: https://onlinelibrary.wiley.com/doi/pdf/10.1029/2020EF001616) doi: 10.1029/2020EF001616

Leal Filho, W., Azeiteiro, U. M., Salvia, A. L., Fritzen, B., & Libonati, R. (2021, September). Fire in Paradise: Why the Pantanal is burning. *Environmental Science & Policy*, *123*, 31–34. Retrieved 2023-12-31, from https://www.sciencedirect.com/science/article/pii/S1462901121001258 doi: 10.1016/j.envsci.2021.05.005

Lehner, B., & Döll, P. (2004, August). Development and validation of a global database of lakes, reservoirs and wetlands. *Journal of Hydrology*, *296*(1-4), 1–22. Retrieved 2023-10-20, from https://linkinghub.elsevier.com/retrieve/pii/S0022169404001404 doi: 10.1016/j.jhydrol.2004.03.028

Lehner, B., Verdin, K., & Jarvis, A. (2008). New global hydrography derived from spaceborne elevation data. *Eos, Transactions American Geophysical Union*, *89*(10), 93–94. Retrieved 2023-03-16, from https://onlinelibrary.wiley.com/doi/abs/10.1029/2008EO100001 (_eprint: https://onlinelibrary.wiley.com/doi/pdf/10.1029/2008EO100001) doi: 10.1029/2008EO100001

Li, W., Cardellach, E., Ribó, S., Rius, A., & Zhou, B. (2021, September). First spaceborne demonstration of BeiDou-3 signals for GNSS reflectometry from CYGNSS constellation. *Chinese Journal of Aeronautics*, *34*(9), 1–10. Retrieved 2023-10-30, from https://www.sciencedirect.com/science/article/pii/S100093612030580X doi: 10.1016/j.cja.2020.11.016

Lin, X., Peng, S., Ciais, P., Hauglustaine, D., Lan, X., Liu, G., ... Zheng, B. (2023, September). Recent methane surges reveal heightened emissions from tropical inundated areas. *EarthArXiv*. Retrieved 2023-12-20, from https://eartharxiv.org/repository/view/5895/

Liu, X., & Zhuang, Q. (2023). Methane emissions from arctic landscapes during 2000–2015: an analysis with land and lake biogeochemistry models. *Biogeosciences*, *20*(6), 1181–1193. Retrieved from https://bg.copernicus.org/articles/20/1181/2023/ doi: 10.5194/bg-20-1181-2023

Lunt, M. F., Palmer, P. I., Feng, L., Taylor, C. M., Boesch, H., & Parker, R. J. (2019, December). An increase in methane emissions from tropical Africa between 2010 and 2016 inferred from satellite data. *Atmospheric Chemistry and Physics*, *19*(23), 14721–14740. Retrieved 2023-03-22, from https://acp.copernicus.org/articles/19/14721/2019/ doi: 10.5194/acp-19-14721-2019

Marques, J. F., Alves, M. B., Silveira, C. F., Amaral e Silva, A., Silva, T. A., dos Santos, V. J., & Calijuri, M. L. (2021, December). Fires dynamics in the Pantanal: Impacts of anthropogenic activities and climate change. *Journal of Environmental Management*, *299*, 113586. Retrieved 2023-12-31, from https://www.sciencedirect.com/science/article/pii/S0301479721016480 doi: 10.1016/j.jenvman.2021.113586

Martin, D. A. (2016, June). At the nexus of fire, water and society. *Philosophical Transactions of the Royal Society B: Biological Sciences*, *371*(1696), 20150172. Retrieved 2023-12-31, from https://royalsocietypublishing.org/doi/full/10.1098/rstb.2015.0172 (Publisher: Royal Society) doi: 10.1098/rstb.2015.0172

Martins, V. S., Novo, E. M. L. M., Lyapustin, A., Aragão, L. E. O. C., Freitas, S. R., & Barbosa, C. C. F. (2018, November). Seasonal and interannual assessment of cloud cover and atmospheric constituents across the Amazon (2000–2015): Insights for

remote sensing and climate analysis. *ISPRS Journal of Photogrammetry and Remote Sensing*, *145*, 309–327. Retrieved 2023-10-26, from https://www.sciencedirect.com/science/article/pii/S0924271618301461 doi: 10.1016/j.isprsjprs.2018.05.013

Masek, J. G., Wulder, M. A., Markham, B., McCorkel, J., Crawford, C. J., Storey, J., & Jenstrom, D. T. (2020, October). Landsat 9: Empowering open science and applications through continuity. *Remote Sensing of Environment*, *248*, 111968. Retrieved 2023-10-25, from https://www.sciencedirect.com/science/article/pii/S0034425720303382 doi: 10.1016/j.rse.2020.111968

Melack, J. M., Basso, L. S., Fleischmann, A. S., Botía, S., Guo, M., Zhou, W., ... MacIntyre, S. (2022). Challenges Regionalizing Methane Emissions Using Aquatic Environments in the Amazon Basin as Examples. *Frontiers in Environmental Science*, *10*. Retrieved 2023-12-18, from https://www.frontiersin.org/articles/10.3389/fenvs.2022.866082

Mgbemene, C. A., Nnaji, C. C., & Nwozor, C. (2016). Industrialization and its backlash: focus on climate change and its consequences. *Journal of Environmental Science and Technology*, *9*(4), 301–316. Retrieved 2023-10-26, from https://www.cabdirect.org/cabdirect/abstract/20163290084 (Publisher: Asian Network for Scientific Information)

Morris, M., Chew, C., Reager, J. T., Shah, R., & Zuffada, C. (2019, November). A novel approach to monitoring wetland dynamics using CYGNSS: Everglades case study. *Remote Sensing of Environment*, *233*, 111417. Retrieved 2023-10-30, from https://www.sciencedirect.com/science/article/pii/S0034425719304365 doi: 10.1016/j.rse.2019.111417

Palmer, S. C. J., Kutser, T., & Hunter, P. D. (2015, February). Remote sensing of inland waters: Challenges, progress and future directions. *Remote Sensing of Environment*, *157*, 1–8. Retrieved 2023-09-26, from https://www.sciencedirect.com/science/article/pii/S0034425714003666 doi: 10.1016/j.rse.2014.09.021

Parker, R. J., Boesch, H., McNorton, J., Comyn-Platt, E., Gloor, M., Wilson, C., ... Bloom, A. A. (2018, June). Evaluating year-to-year anomalies in tropical wetland methane emissions using satellite CH4 observations. *Remote Sensing of Environment*, *211*, 261–275. Retrieved 2023-09-26, from https://www.sciencedirect.com/science/article/pii/S0034425718300178 doi: 10.1016/j.rse.2018.02.011

Pekel, J.-F., Cottam, A., Gorelick, N., & Belward, A. S. (2016, December). High-resolution mapping of global surface water and its long-term changes. *Nature*, *540*(7633), 418–422. Retrieved 2023-10-20, from https://www.nature.com/articles/nature20584 (Number: 7633 Publisher: Nature Publishing Group) doi: 10.1038/nature20584

Prigent, C., Jimenez, C., & Bousquet, P. (2020). Satellite-Derived Global Surface Water Extent and Dynamics Over the Last 25 Years (GIEMS-2). *Journal of Geophysical Research: Atmospheres*, *125*(3), e2019JD030711. Retrieved 2023-09-26, from https://onlinelibrary.wiley.com/doi/abs/10.1029/2019JD030711 (_eprint: https://onlinelibrary.wiley.com/doi/pdf/10.1029/2019JD030711) doi: 10.1029/2019JD030711

Prigent, C., Matthews, E., Aires, F., & Rossow, W. B. (2001). Remote sensing of global wetland dynamics with multiple satellite data sets. *Geophysical Research Letters*, *28*(24), 4631–4634. Retrieved 2023-09-26, from https://onlinelibrary.wiley.com/doi/abs/10.1029/2001GL013263 (_eprint: https://onlinelibrary.wiley.com/doi/pdf/10.1029/2001GL013263) doi: 10.1029/2001GL013263

Prigent, C., Papa, F., Aires, F., Rossow, W. B., & Matthews, E. (2007). Global inundation dynamics inferred from multiple satellite observations, 1993–2000. *Journal of Geophysical Research: Atmospheres*, *112*(D12). Retrieved 2023-10-23, from https://onlinelibrary.wiley.com/doi/abs/10.1029/2006JD007847 (_eprint: https://onlinelibrary.wiley.com/doi/pdf/10.1029/2006JD007847) doi: 10.1029/2006JD007847

Rinaldo, A., Rigon, R., Banavar, J. R., Maritan, A., & Rodriguez-Iturbe, I. (2014, February). Evolution and selection of river networks: Statics, dynamics, and complexity. *Proceedings of the National Academy of Sciences*, *111*(7), 2417–2424. Retrieved 2023-12-20, from https://pnas.org/doi/full/10.1073/pnas.1322700111 doi: 10.1073/pnas.1322700111

Ruf, C. (2022). *Cygnss handbook 2022*. doi: 10.3998/mpub.12741920

Ruf, C. S. (2022). *CYGNSS Handbook*. Michigan Publishing Services. Retrieved 2023-03-16, from https://www.fulcrum.org/concern/monographs/g445cg50v?locale=en#toc doi: 10.3998/mpub.12741920

Ruf, C. S., Atlas, R., Chang, P. S., Clarizia, M. P., Garrison, J. L., Gleason, S., ... Zavorotny, V. U. (2016, March). New Ocean Winds Satellite Mission to Probe Hurricanes and Tropical Convection. *Bulletin of the American Meteorological Society*, *97*(3), 385–395. Retrieved 2023-10-28, from https://journals.ametsoc.org/view/journals/bams/97/3/bams-d-14-00218.1.xml (Publisher: American Meteorological Society Section: Bulletin of the American Meteorological Society) doi: 10.1175/BAMS-D-14-00218.1

Ruf, C. S., Chew, C., Lang, T., Morris, M. G., Nave, K., Ridley, A., & Balasubramaniam, R. (2018, June). A New Paradigm in Earth Environmental Monitoring with the CYGNSS Small Satellite Constellation. *Scientific Reports*, *8*(1), 8782. Retrieved 2023-10-28, from https://www.nature.com/articles/s41598-018-27127-4 (Number: 1 Publisher: Nature Publishing Group) doi: 10.1038/s41598-018-27127-4

Runge, C. A., Watson, J. E. M., Butchart, S. H. M., Hanson, J. O., Possingham, H. P., & Fuller, R. A. (2015, December). Protected areas and global conservation of migratory birds. *Science*, *350*(6265), 1255–1258. Retrieved 2023-12-31, from https://www.science.org/doi/full/10.1126/science.aac9180 (Publisher: American Association for the Advancement of Science) doi: 10.1126/science.aac9180

Saunois, M., Stavert, A. R., Poulter, B., Bousquet, P., Canadell, J. G., Jackson, R. B., ... Zhuang, Q. (2020, July). The Global Methane Budget 2000–2017. *Earth System Science Data*, *12*(3), 1561–1623. Retrieved 2023-09-26, from https://essd.copernicus.org/articles/12/1561/2020/ (Publisher: Copernicus GmbH) doi: 10.5194/essd-12-1561-2020

Sayre, R. (2022). *World terrestrial ecosystems (WTE) 2020*. U.S. Geological Survey. Retrieved 2023-05-05, from https://www.sciencebase.gov/catalog/item/6296791ed34ec53d276bb293 (Type: dataset) doi: 10.5066/P9DO61LP

Senyurek, V., Lei, F., Boyd, D., Kurum, M., Gurbuz, A. C., & Moorhead, R. (2020, January). Machine Learning-Based CYGNSS Soil Moisture Estimates over ISMN sites in CONUS. *Remote Sensing*, *12*(7), 1168. Retrieved 2023-10-30, from https://www.mdpi.com/2072-4292/12/7/1168 (Number: 7 Publisher: Multidisciplinary Digital Publishing Institute) doi: 10.3390/rs12071168

Skeie, R. B., Hodnebrog, Ø., & Myhre, G. (2023). Trends in atmospheric methane concentrations since 1990 were driven and modified by anthropogenic emissions. *Communications Earth & Environment*, *4*(1), 317. Retrieved from https://doi.org/10.1038/s43247-023-00969-1 doi: 10.1038/s43247-023-00969-1

Somveille, M., Manica, A., Butchart, S. H. M., & Rodrigues, A. S. L. (2013, August). Mapping Global Diversity Patterns for Migratory Birds. *PLOS ONE*, *8*(8), e70907. Retrieved 2023-12-31, from https://journals.plos.org/plosone/article?id=10.1371/journal.pone.0070907 (Publisher: Public Library of Science) doi: 10.1371/journal.pone.0070907

Thiery, W., Lange, S., Rogelj, J., Schleussner, C.-F., Gudmundsson, L., Seneviratne, S. I., ... Wada, Y. (2021, October). Intergenerational inequities in exposure to climate extremes. *Science*, *374*(6564), 158–160. Retrieved 2023-10-23, from https://www.science.org/doi/10.1126/science.abi7339 (Publisher: American Association for the Advancement of Science) doi: 10.1126/science.abi7339

Topp, S. N., Pavelsky, T. M., Jensen, D., Simard, M., & Ross, M. R. V. (2020, January). Research Trends in the Use of Remote Sensing for Inland Water Quality Science:

Moving Towards Multidisciplinary Applications. *Water*, *12*(1), 169. Retrieved 2023-10-16, from https://www.mdpi.com/2073-4441/12/1/169 (Number: 1 Publisher: Multidisciplinary Digital Publishing Institute) doi: 10.3390/w12010169

Trenberth, K. E., Fasullo, J. T., & Shepherd, T. G. (2015, August). Attribution of climate extreme events. *Nature Climate Change*, *5*(8), 725–730. Retrieved 2023-10-23, from https://www.nature.com/articles/nclimate2657 (Number: 8 Publisher: Nature Publishing Group) doi: 10.1038/nclimate2657

UNESCO. (2020). *The United Nations World Water Development Report 2020 :: water and climate change*. UNESCO,. Retrieved 2023-10-24, from https://digitallibrary.un.org/record/3892703

Unwin, M. J., Pierdicca, N., Cardellach, E., Rautiainen, K., Foti, G., Blunt, P., ... Tossaint, M. (2021). An Introduction to the HydroGNSS GNSS Reflectometry Remote Sensing Mission. *IEEE Journal of Selected Topics in Applied Earth Observations and Remote Sensing*, *14*, 6987–6999. Retrieved 2023-10-30, from https://ieeexplore.ieee.org/document/9456091 (Conference Name: IEEE Journal of Selected Topics in Applied Earth Observations and Remote Sensing) doi: 10.1109/JSTARS.2021.3089550

van der Walt, S., Schönberger, J. L., Nunez-Iglesias, J., Boulogne, F., Warner, J. D., Yager, N., ... scikit-image contributors (2014). scikit-image: image processing in python. *PeerJ*, *2*, e453. doi: 10.7717/peerj.453

Wan, W., Liu, B., Zeng, Z., Chen, X., Wu, G., Xu, L., ... Hong, Y. (2019, January). Using CYGNSS Data to Monitor China's Flood Inundation during Typhoon and Extreme Precipitation Events in 2017. *Remote Sensing*, *11*(7), 854. Retrieved 2023-10-30, from https://www.mdpi.com/2072-4292/11/7/854 (Number: 7 Publisher: Multidisciplinary Digital Publishing Institute) doi: 10.3390/rs11070854

Williams-Jara, G. M., Espinoza-Tenorio, A., Monzón-Alvarado, C., Posada-Vanegas, G., & Infante-Mata, D. (2022, July). Fires in coastal wetlands: a review of research trends and management opportunities. *Wetlands*, *42*(6), 56. Retrieved 2023-12-31, from https://doi.org/10.1007/s13157-022-01576-0 doi: 10.1007/s13157-022-01576-0

Wood, E. F., Roundy, J. K., Troy, T. J., van Beek, L. P. H., Bierkens, M. F. P., Blyth, E., ... Whitehead, P. (2011). Hyperresolution global land surface modeling: Meeting a grand challenge for monitoring Earth's terrestrial water. *Water Resources Research*, *47*(5). Retrieved 2023-10-24, from https://onlinelibrary.wiley.com/doi/abs/10.1029/2010WR010090 (_eprint: https://onlinelibrary.wiley.com/doi/pdf/10.1029/2010WR010090) doi: 10.1029/2010WR010090

Xi, X., Zhuang, Q., Kim, S., & Zhang, Z. (2023). Methane emissions from land and aquatic ecosystems in western siberia: An analysis with methane biogeochemistry models. *Journal of Geophysical Research: Biogeosciences*, *128*(7), e2023JG007466. Retrieved from https://agupubs.onlinelibrary.wiley.com/doi/abs/10.1029/2023JG007466 (e2023JG007466 2023JG007466) doi: https://doi.org/10.1029/2023JG007466

Yan, Q., Huang, W., Jin, S., & Jia, Y. (2020, September). Pan-tropical soil moisture mapping based on a three-layer model from CYGNSS GNSS-R data. *Remote Sensing of Environment*, *247*, 111944. Retrieved 2023-10-30, from https://www.sciencedirect.com/science/article/pii/S003442572030314X doi: 10.1016/j.rse.2020.111944

Zedler, J. B., & Kercher, S. (2005). WETLAND RESOURCES: Status, Trends, Ecosystem Services, and Restorability. *Annual Review of Environment and Resources*, *30*(1), 39–74. Retrieved 2023-12-31, from https://doi.org/10.1146/annurev.energy.30.050504.144248 (_eprint: https://doi.org/10.1146/annurev.energy.30.050504.144248) doi: 10.1146/annurev.energy.30.050504.144248

Zeiger, P., Frappart, F., Darrozes, J., Prigent, C., & Jiménez, C. (2022, December). Analysis of CYGNSS coherent reflectivity over land for the characterization of pan-tropical inundation dynamics. *Remote Sensing of Environment*, *282*, 113278. Retrieved 2023-10-30, from https://www.sciencedirect.com/science/article/pii/

S0034425722003844 doi: 10.1016/j.rse.2022.113278

Zhang, S., Ma, Z., Li, Z., Zhang, P., Liu, Q., Nan, Y., ... Zhao, H. (2021, January). Using CYGNSS Data to Map Flood Inundation during the 2021 Extreme Precipitation in Henan Province, China. *Remote Sensing*, *13*(24), 5181. Retrieved 2023-10-30, from https://www.mdpi.com/2072-4292/13/24/5181 (Number: 24 Publisher: Multidisciplinary Digital Publishing Institute) doi: 10.3390/rs13245181

Zhang, Z., Fluet-Chouinard, E., Jensen, K., McDonald, K., Hugelius, G., Gumbricht, T., ... Poulter, B. (2021a, October). *Development of a global dataset of Wetland Area and Dynamics for Methane Modeling (WAD2M).* Zenodo. Retrieved from https://doi.org/10.5281/zenodo.5553187 doi: 10.5281/zenodo.5553187

Zhang, Z., Fluet-Chouinard, E., Jensen, K., McDonald, K., Hugelius, G., Gumbricht, T., ... Poulter, B. (2021b, May). Development of the global dataset of Wetland Area and Dynamics for Methane Modeling (WAD2M). *Earth System Science Data*, *13*(5), 2001–2023. Retrieved 2023-09-26, from https://essd.copernicus.org/articles/13/2001/2021/ (Publisher: Copernicus GmbH) doi: 10.5194/essd-13-2001-2021

Zhang, Z., Poulter, B., Feldman, A. F., Ying, Q., Ciais, P., Peng, S., & Li, X. (2023). Recent intensification of wetland methane feedback. *Nature Climate Change*, *13*(5), 430–433. Retrieved from https://doi.org/10.1038/s41558-023-01629-0 doi: 10.1038/s41558-023-01629-0

Zhang, Z., Zimmermann, N. E., Stenke, A., Li, X., Hodson, E. L., Zhu, G., ... Poulter, B. (2017, September). Emerging role of wetland methane emissions in driving 21st century climate change. *Proceedings of the National Academy of Sciences*, *114*(36), 9647–9652. Retrieved 2023-10-24, from https://www.pnas.org/doi/full/10.1073/pnas.1618765114 (Publisher: Proceedings of the National Academy of Sciences) doi: 10.1073/pnas.1618765114

Figure 1.

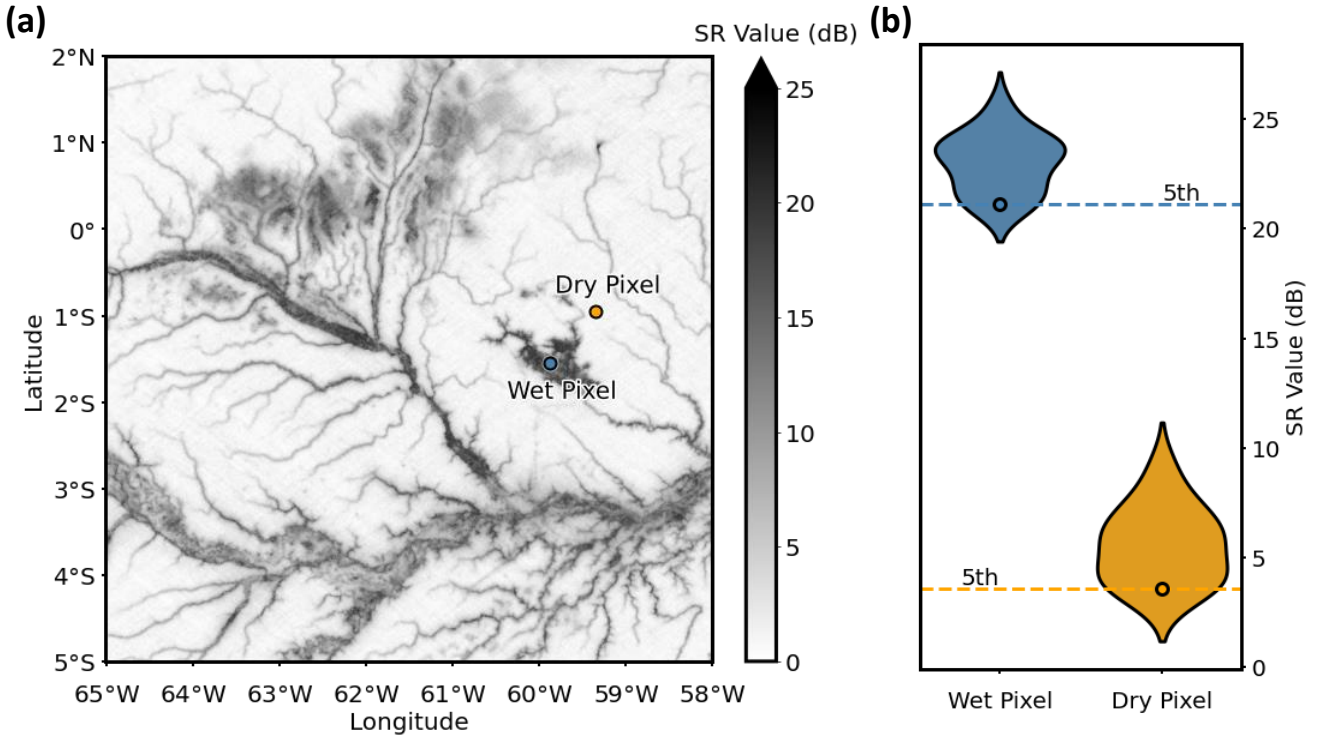
(a)
SR Value (dB)
25
20
15
10
5
0
2°N
1°N
0°
1°S
2°S
3°S
4°S
5°S
Latitude
Dry Pixel
Wet Pixel
65°W
64°W
63°W
62°W
61°W
60°W
59°W
58°W
Longitude
(b)
5th
5th
SR Value (dB)
Wet Pixel
Dry Pixel

Figure 2.

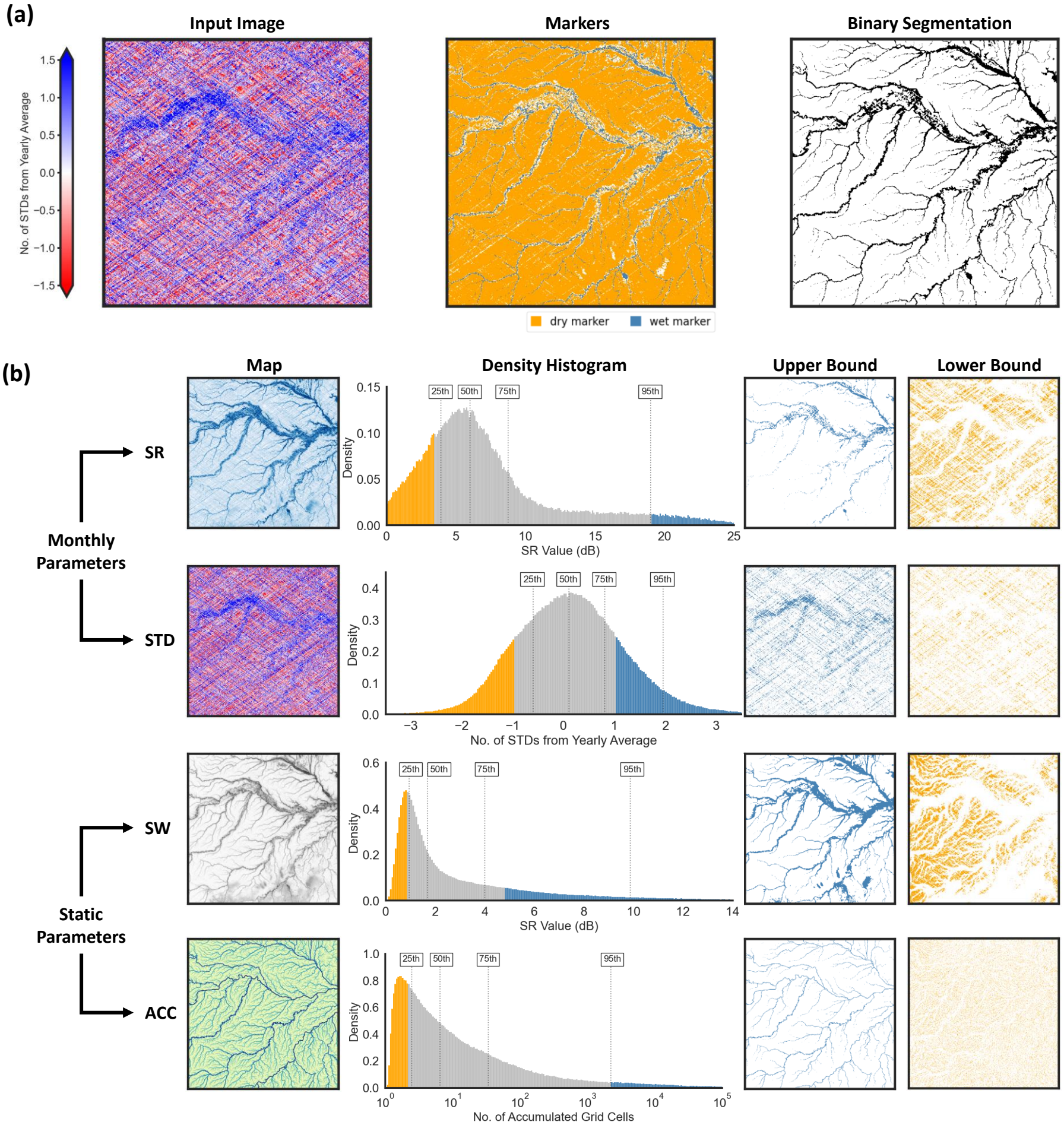
(a)
Input Image
Markers
Binary Segmentation
No. of STDs from Yearly Average
1.5
1.0
0.5
0.0
−0.5
−1.0
−1.5
dry marker
wet marker
(b)
Map
Density Histogram
Upper Bound
Lower Bound
SR
STD
SW
ACC
Monthly Parameters
Static Parameters
25th
50th
75th
95th
Density
SR Value (dB)
No. of STDs from Yearly Average
No. of Accumulated Grid Cells

Figure 3.

(a)

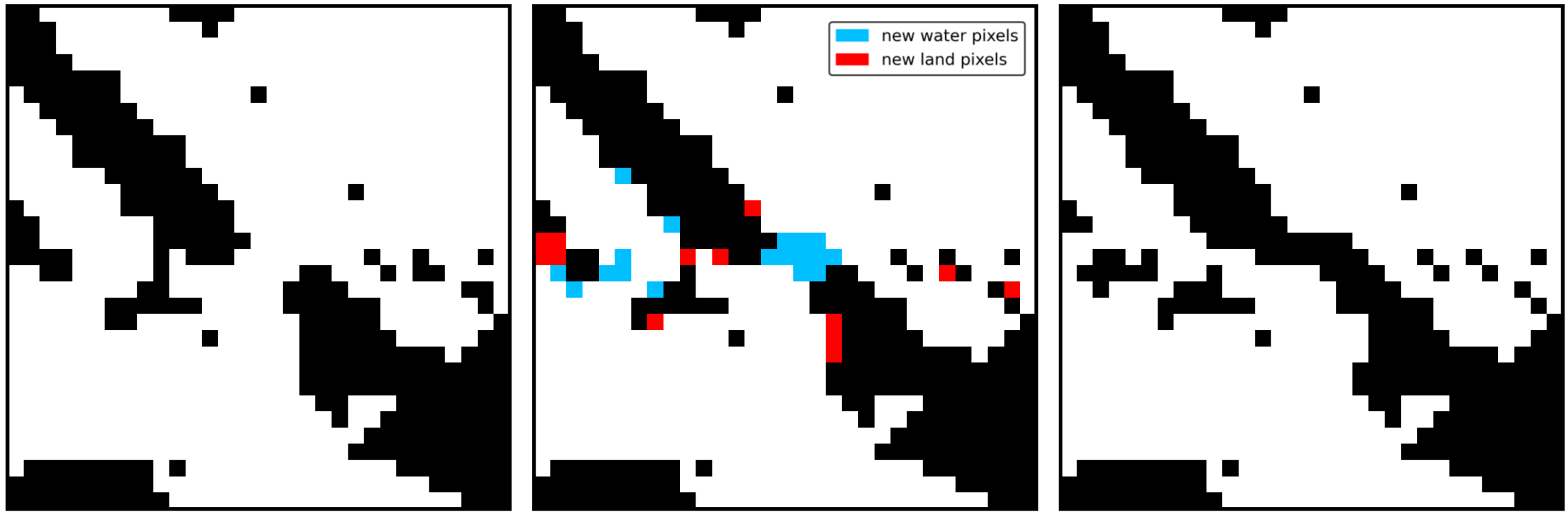
Segmentaion
Changes
Improved Segmentaion
new water pixels
new land pixels

(b)

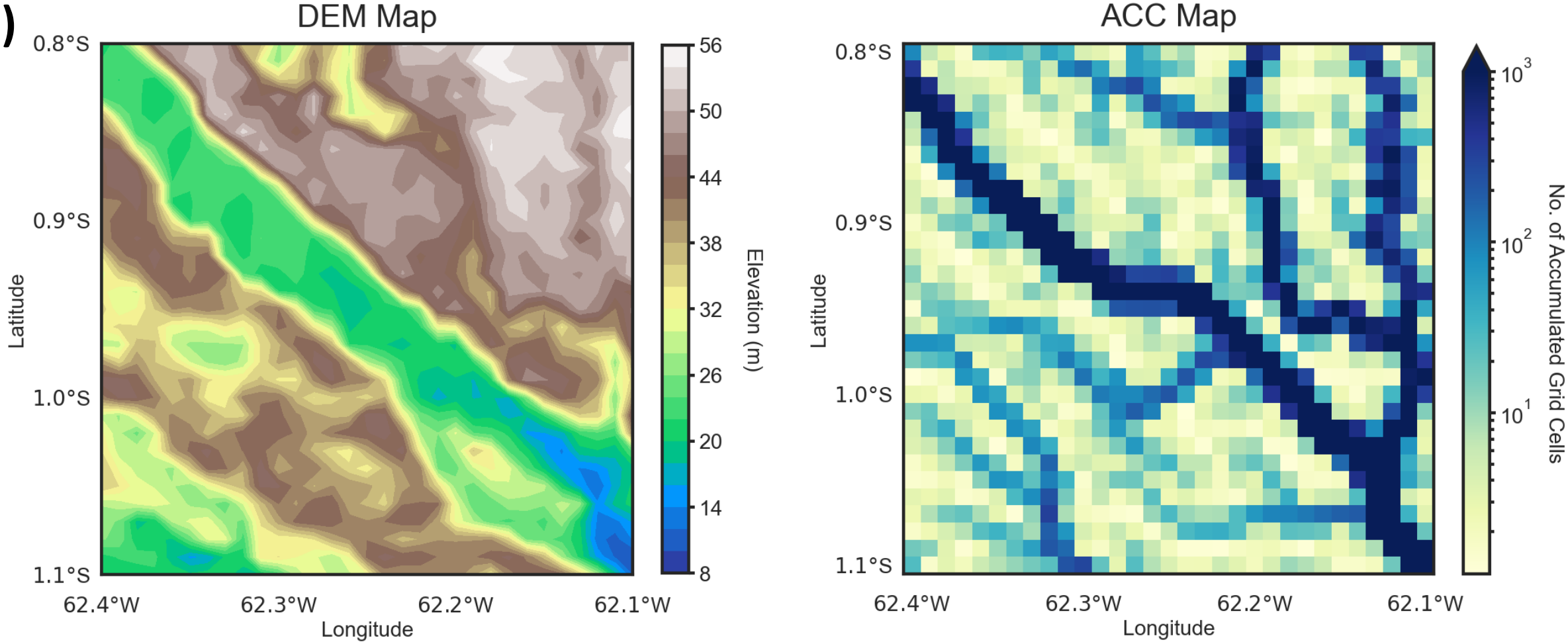
DEM Map
ACC Map
0.8°S
0.9°S
1.0°S
1.1°S
Latitude
62.4°W
62.3°W
62.2°W
62.1°W
Longitude
56
50
44
38
32
26
20
14
8
Elevation (m)
10^3
10^2
10^1
No. of Accumulated Grid Cells

Figure 4.

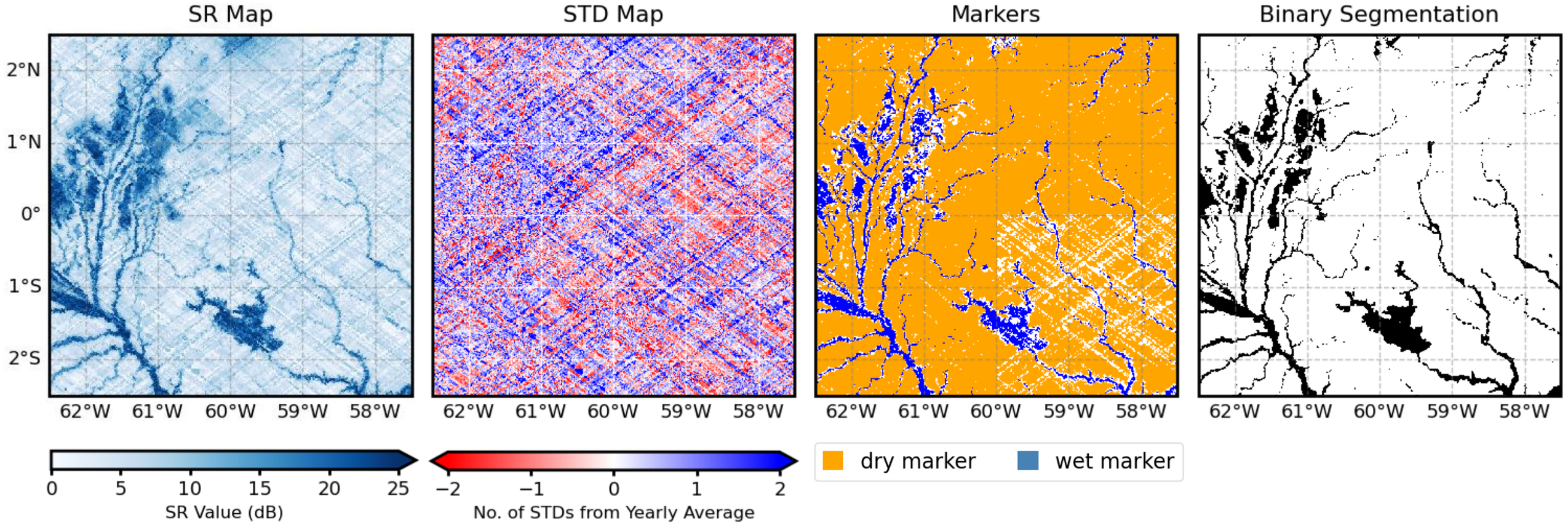
SR Map
STD Map
Markers
Binary Segmentation
2°N
1°N
0°
1°S
2°S
62°W
61°W
60°W
59°W
58°W
0
5
10
15
20
25
SR Value (dB)
−2
−1
0
1
2
No. of STDs from Yearly Average
dry marker
wet marker

Figure 5.

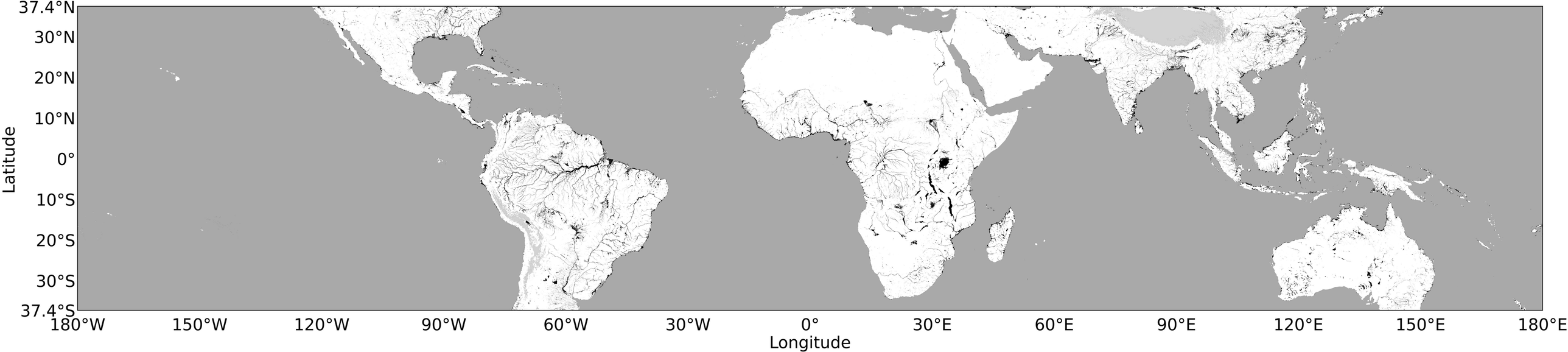
37.4°N
30°N
20°N
10°N
0°
10°S
20°S
30°S
37.4°S
Latitude
180°W
150°W
120°W
90°W
60°W
30°W
0°
30°E
60°E
90°E
120°E
150°E
180°E
Longitude

Figure 6.

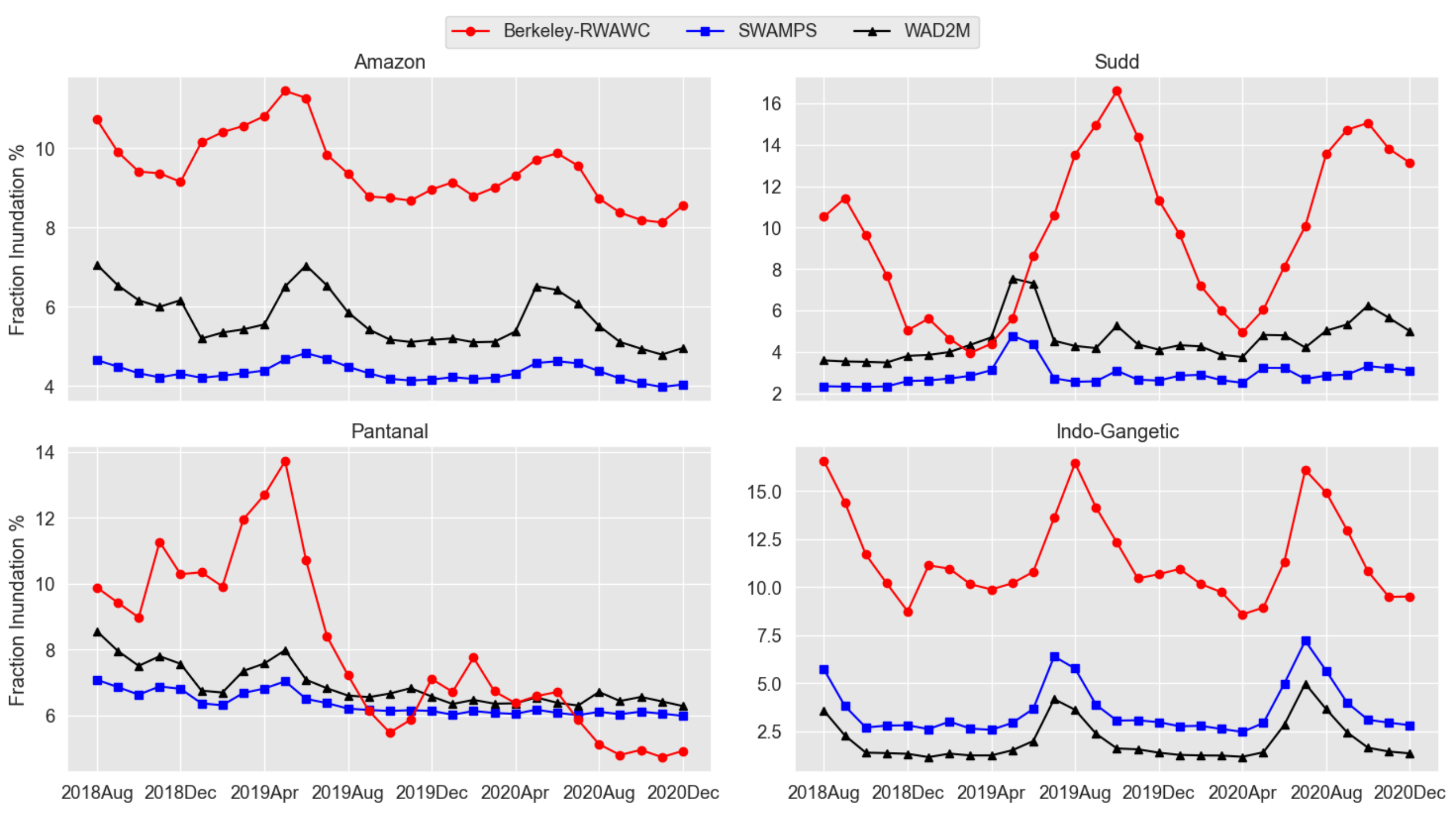
Berkeley-RWAWC
SWAMPS
WAD2M
Amazon
Sudd
Pantanal
Indo-Gangetic
Fraction Inundation %
Fraction Inundation %
2018Aug
2018Dec
2019Apr
2019Aug
2019Dec
2020Apr
2020Aug
2020Dec

Figure 7.

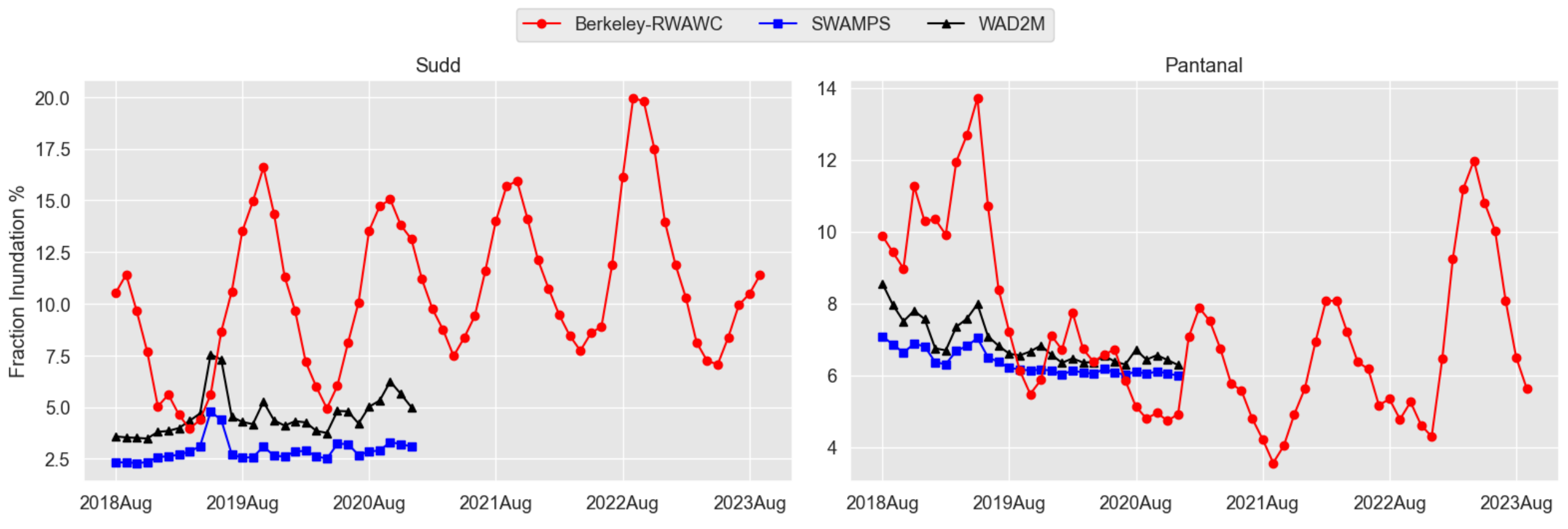
Berkeley-RWAWC
SWAMPS
WAD2M
Sudd
Pantanal
Fraction Inundation %
20.0
17.5
15.0
12.5
10.0
7.5
5.0
2.5
14
12
10
8
6
4
2018Aug
2019Aug
2020Aug
2021Aug
2022Aug
2023Aug